

11-1-2017

Mitochondrial Reactive Oxygen Species in Lipotoxic Hearts Induces Post-Translational Modifications of AKAP121, DRP1 and OPA1 That Promote Mitochondrial Fission

Kensuke Tsushima

University of Iowa

Heiko Bugger

University of Utah School of Medicine, heiko.bugger@universitaets-herzzentrum.de

Adam R. Wende

University of Utah School of Medicine, arwende@uab.edu


Jamie Soto

University of Iowa, jamie-soto@uiowa.edu

Gregory A. Jenson

Follow this and additional works at: <http://digitalcommons.unl.edu/biochemfacpub>

University of Iowa, greg-jenson@uiowa.edu

 Part of the [Biochemical Phenomena, Metabolism, and Nutrition Commons](#), [Biochemistry Commons](#), [Biotechnology Commons](#), [Cardiology Commons](#), [Circulatory and Respiratory Physiology Commons](#), [Medical Biochemistry Commons](#), and the [Other Biochemistry, Biophysics, and Structural Biology Commons](#)

Tsushima, Kensuke; Bugger, Heiko; Wende, Adam R.; Soto, Jamie; Jenson, Gregory A.; Tor, Austin R.; McGlaflin, Rose; Kenny, Helena C.; Zhang, Yuan; Souvenir, Rhonda; Hu, Xiao X.; Sloan, Crystal L.; Pereira, Renata O.; Lira, Vitor A.; Spitzer, Kenneth W.; Sharp, Terry L.; Shoghi, Koresh I.; Sparagna, Genevieve C.; Rog-Zielinska, Eva A.; Kohl, Peter; Khalimonchuk, Oleh; Schaffer, Jean E.; and Abel, E. Dale, "Mitochondrial Reactive Oxygen Species in Lipotoxic Hearts Induces Post-Translational Modifications of AKAP121, DRP1 and OPA1 That Promote Mitochondrial Fission" (2017). *Biochemistry -- Faculty Publications*. 359.
<http://digitalcommons.unl.edu/biochemfacpub/359>

This Article is brought to you for free and open access by the Biochemistry, Department of at DigitalCommons@University of Nebraska - Lincoln. It has been accepted for inclusion in Biochemistry -- Faculty Publications by an authorized administrator of DigitalCommons@University of Nebraska - Lincoln.

Authors

Kensuke Tsushima, Heiko Bugger, Adam R. Wende, Jamie Soto, Gregory A. Jenson, Austin R. Tor, Rose McGlauflin, Helena C. Kenny, Yuan Zhang, Rhonda Souvenir, Xiao X. Hu, Crystal L. Sloan, Renata O. Pereira, Vitor A. Lira, Kenneth W. Spitzer, Terry L. Sharp, Kooresh I. Shoghi, Genevieve C. Sparagna, Eva A. Rog-Zielinska, Peter Kohl, Oleh Khalimonchuk, Jean E. Schaffer, and E. Dale Abel

Mitochondrial Reactive Oxygen Species in Lipotoxic Hearts Induces Post-Translational Modifications of AKAP121, DRP1 and OPA1 That Promote Mitochondrial Fission

Kensuke Tsushima^{1,2*}

Heiko Bugger^{2,3*}

Adam R. Wende^{2,4}

Jamie Soto^{1,2}

Gregory A. Jenson¹

Austin R. Tor¹

Rose McGlaufflin¹

Helena C. Kenny¹

Yuan Zhang¹

Rhonda Souvenir¹

Xiao X. Hu²

Crystal L. Sloan²

Renata O. Pereira¹

Vitor A Lira⁵

Kenneth W. Spitzer⁶

Terry L. Sharp⁷

Kooresh I. Shoghi⁷

Genevieve C. Sparagna⁸

Eva A. Rog-Zielinska⁹

Peter Kohl⁹

Oleh Khalimonchuk^{10,11}

Jean E. Schaffer¹²

E. Dale Abel^{1,2}

1 Fraternal Order of Eagles Diabetes Research Center, Division of Endocrinology and Metabolism, Roy J. and Lucille A. Carver College of Medicine, University of Iowa, Iowa City, IA, USA

2 Division of Endocrinology, Metabolism, and Diabetes and Program in Molecular Medicine, University of Utah School of Medicine, Salt Lake City, UT, USA

3 Heart Center, Cardiology and Angiology I, Faculty of Medicine, University of Freiburg, Freiburg, Germany

4 Division of Molecular and Cellular Pathology, Department of Pathology, University of Alabama at Birmingham, Birmingham, AL, USA

5 Department of Health and Human Physiology, University of Iowa, Iowa City, IA, USA

6 Nora Eccles Harrison Cardiovascular Research and Training Institute, University of Utah School of Medicine, Salt Lake City, UT, USA

7 Department of Radiology, Washington University School of Medicine, St. Louis, MO, USA

8 Department of Medicine/Division of Cardiology, University of Colorado Anschutz Medical Center, Aurora, CO, USA

9 Institute for Experimental Cardiovascular Medicine, University Heart Centre, Faculty of Medicine, University of Freiburg, Freiburg, Germany,

10 Department of Biochemistry, University of Utah School of Medicine, Salt Lake City, UT, USA

11 Department of Biochemistry, and Nebraska Redox Biology Center, University of Nebraska, Lincoln, NE, USA

12 Diabetic Cardiovascular Disease Center, Cardiovascular Division, Washington University School of Medicine, St. Louis, MO, USA

Corresponding author: Dr. E. Dale Abel
Fraternal Order of Eagles Diabetes Research Center
Division of Endocrinology and Metabolism
Roy J. and Lucille A. Carver College of Medicine
University of Iowa
4312 PBDB, 169 Newton Road
Iowa City, IA 52242-1101
Tel: 319-353-3050 Fax: 319-335-8327
DRAdmin@uiowa.edu

* Kensuke Tsushima and Heiko Bugger contributed equally to this work and are considered co-first authors.

Abstract

Rationale: Cardiac lipotoxicity, characterized by increased uptake, oxidation and accumulation of lipid intermediates, contributes to cardiac dysfunction in obesity and diabetes. However, mechanisms linking lipid overload and mitochondrial dysfunction are incompletely understood.

Objective: To elucidate the mechanisms for mitochondrial adaptations to lipid overload in postnatal hearts *in vivo*.

Methods and Results: Using a transgenic mouse model of cardiac lipotoxicity overexpressing long-chain acyl-CoA synthetase 1 in cardiomyocytes, we show that modestly increased myocardial fatty acid uptake leads to mitochondrial structural remodeling with significant reduction in minimum diameter. This is associated with increased palmitoyl-carnitine oxidation and increased reactive oxygen species (ROS) generation in isolated mitochondria. Mitochondrial morphological changes and elevated ROS generation are also observed in palmitate-treated neonatal rat ventricular cardiomyocytes (NRVCs). Palmitate exposure to NRVCs initially activates mitochondrial respiration, coupled with increased mitochondrial membrane potential and adenosine triphosphate (ATP) synthesis. However, long-term exposure to palmitate (>8h) enhances ROS generation, which is accompanied by loss of the mitochondrial reticulum and a pattern suggesting increased mitochondrial fission. Mechanistically, lipid-induced changes in mitochondrial redox status increased mitochondrial fission by increased ubiquitination of A-kinase anchor protein (AKAP121) leading to reduced phosphorylation of DRP1 at Ser637 and altered proteolytic processing of OPA1. Scavenging mitochondrial ROS restored mitochondrial morphology *in vivo* and *in vitro*.

Conclusions: Our results reveal a molecular mechanism by which lipid overload-induced mitochondrial ROS generation causes mitochondrial dysfunction by inducing post-translational modifications of mitochondrial proteins that regulate mitochondrial dynamics. These findings provide a novel mechanism for mitochondrial dysfunction in lipotoxic cardiomyopathy.

Keywords: Cardiac lipotoxicity, mitochondrial dynamics, oxidative stress, heart failure, diabetic cardiomyopathy, metabolism, reactive oxygen species, lipids and cholesterol, pathophysiology

Nonstandard Abbreviations and Acronyms:

4HNE	4-hydroxy-2-nonenal
ACSL1	Long-chain acyl-CoA synthetase 1
ACTA1	alpha skeletal muscle actin
AKAP121	A-kinase anchor protein 121
ATP	Adenosine triphosphate
BNP	B-type natriuretic peptide
BSA	Bovine serum albumin
CDK1	Cyclin-dependent kinase 1
CPT1	Carnitine palmitoyl transferase I
DAG	Diacylglycerol
DCFDA	2',7'-dichlorofluorescein-diacetate
DES1	Dihydroceramide desaturase 1
DRP1	Dynamin related protein 1
FA	Fatty acid
IVS	Interventricular septum
L4CL	Tetra-linoleic cardiolipin
LCAD	Long-chain acyl-CoA dehydrogenase
LVEDV	Left-ventricular end-diastolic volume
LVEF	Left-ventricular ejection fraction
MCAD	Medium-chain acyl-CoA dehydrogenase
Mfn	Mitofusin
NRVC	Neonatal rat ventricular cardiomyocyte
OCR	Oxygen consumption rate
OPA1	Optic atrophy 1
OXPHOS	Oxidative phosphorylation
PAGE	Polyacrylamide gel electrophoresis
PPAR	Peroxisome proliferator-activated receptor
ROS	Reactive oxygen species
SOD2	Superoxide dismutase 2
UPS	ubiquitin-proteasome system
VDAC	Voltage-dependent anion channel

Introduction

To maintain high energy requirements for contractile function, the heart requires an uninterrupted delivery of oxygen and substrates that are oxidized to promote adenosine triphosphate (ATP) synthesis. ATP consumption primarily fuels sarcomere contraction and ionic pumps that maintain membrane potential.¹ In the healthy well-oxygenated heart, mitochondria are central to cardiomyocyte energy metabolism.¹ Mitochondrial oxidation of fatty acids (FAs), glucose, ketone bodies and lactate accounts for the majority of ATP generation in cardiomyocytes. FAs derived from circulating triglyceride-rich lipoproteins and albumin bound non-esterified FAs are oxidized in the mitochondrial matrix via β -oxidation, whereas pyruvate derived from glucose and lactate is oxidized by the pyruvate-dehydrogenase complex, localized within the inner mitochondrial membrane. Acetyl-CoA formed from FAs and pyruvate is oxidized within the mitochondrial matrix by the citric acid cycle. Healthy adult cardiomyocytes preferentially utilize fatty acids as an energy substrate.²⁻⁴ However, energy substrate usage is flexible in normal hearts and varies to adapt to physiological or pathological stresses.⁵

Diabetes and insulin resistance are the most common metabolic disorders in the world. Cardiovascular complications are the main cause of death from diabetes mellitus, given the high prevalence of comorbid risk factors, such as coronary artery disease. In addition, diabetes mellitus increases the risk for heart failure by mechanisms that may be independent of underlying myocardial ischemia or hypertension.⁶ This increased vulnerability termed "*diabetic cardiomyopathy*", has a complex pathophysiology that includes altered myocardial substrate utilization.^{7, 8} An important characteristic of the metabolic abnormality in diabetic hearts is "metabolic inflexibility", characterized by reduced glucose utilization and increased FA utilization. An imbalance between substrate uptake and utilization

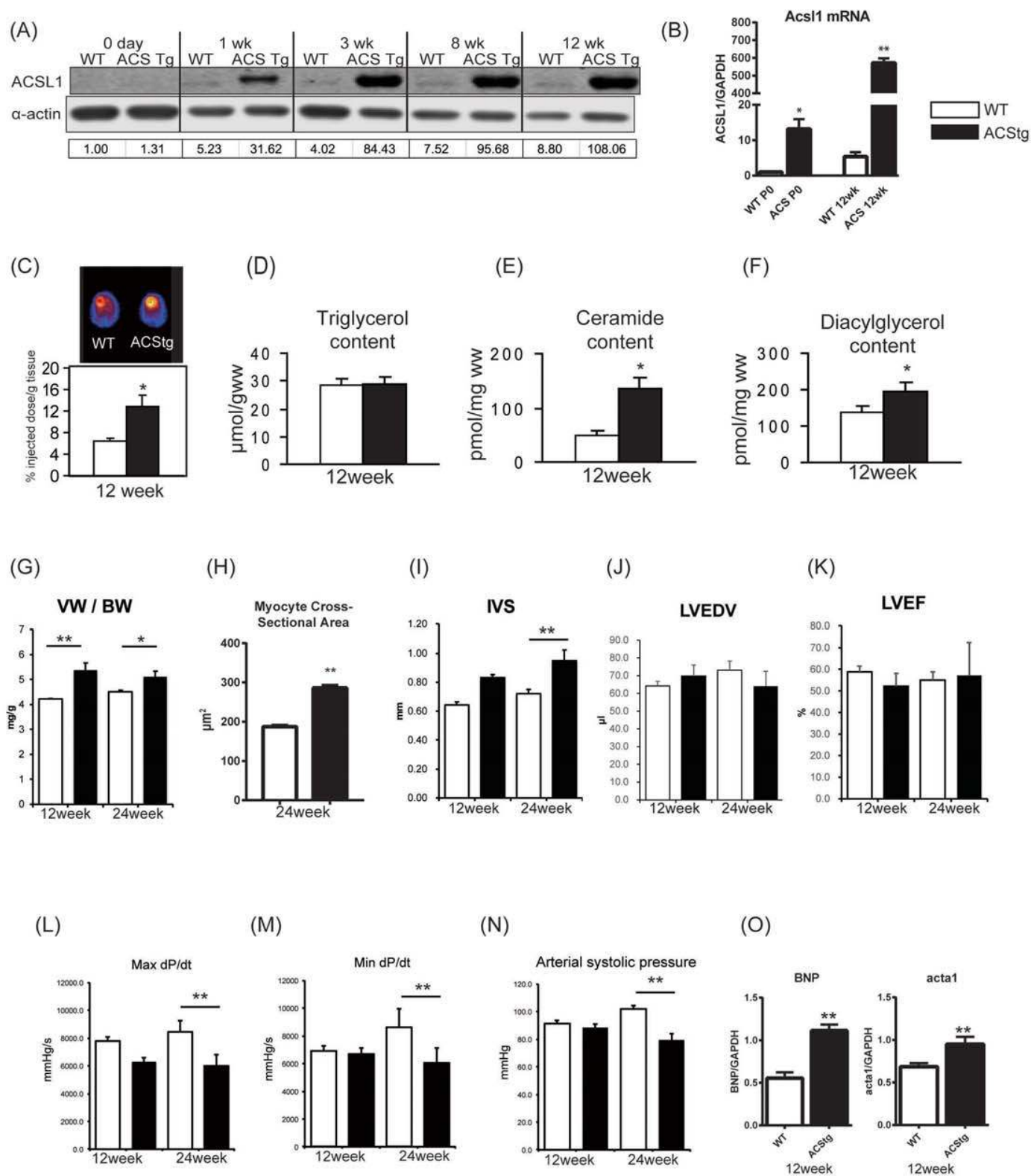
may lead to the accumulation of toxic metabolic intermediates.⁹ Studies by us and others reveal that, in addition to altered substrate utilization, diabetes or myocardial insulin resistance impairs mitochondrial bioenergetics characterized by decreased oxidative capacity, increased ROS generation and mitochondrial uncoupling.¹⁰⁻¹² It is likely that mitochondrial dysfunction is multifactorial, although the relative contributions of increased lipid uptake versus changes in insulin signaling are incompletely understood.

To understand the mechanisms by which increased cardiac lipid uptake could alter mitochondrial function, we investigated mice with cardiomyocyte-restricted low-level overexpression of long chain acyl-CoA synthetase 1 (ACSL1) in which myocardial palmitate biodistribution was moderately increased (2- fold).¹³ In this murine model, the modest increase in FA uptake dramatically remodeled the mitochondrial network, leading to the accumulation of elongated mitochondria with reduced diameter in cardiomyocytes. Similar changes, appearing on 2-D microscopy as numerous "fragmented" mitochondria, were recapitulated in rat neonatal cardiomyocytes (NRVCs) and L6 myotubes following short-term exposure to the long chain FA palmitate. Mechanistically, these changes in mitochondrial morphology reflected changes in mitochondrial dynamics that were mediated via ROS-induced post-translational modification of mitochondrial proteins, AKAP121, DRP1 and OPA1. Thus, lipid overload leads to dysregulation of mitochondrial dynamics, which may impair mitochondrial bioenergetics in diabetic cardiomyopathy.

Methods

The authors declare that all supporting data are available within the article and its supplementary materials. Detailed methods can be found in the supplementary materials.

Figure 1



Results

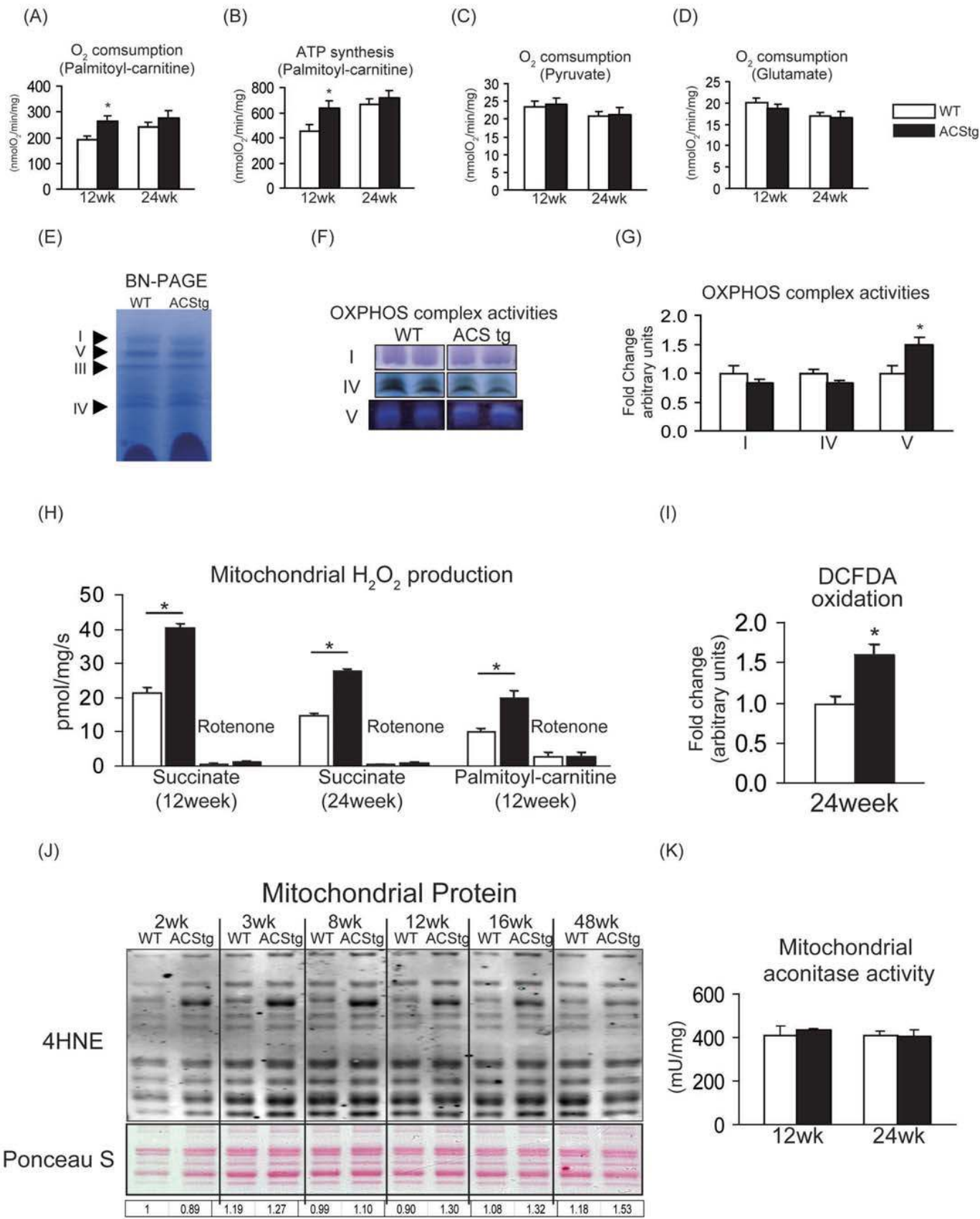
Increased FA uptake elevates myocardial ceramide and diacylglycerol content and induces cardiac hypertrophy and modest systolic dysfunction.

To investigate the consequences of persistent lipid overload in the heart, we examined mice with low-level overexpression of long chain acyl-CoA synthetase 1 (ACSL1) driven by the cardiomyocytespecific α -MHC promoter (ACStg mice). Because our goal was to examine mitochondrial adaptations prior to the onset of lipotoxic cardiomyopathy, we studied the line with the lowest level of ACSL1 overexpression, which does not develop overt heart failure until animals are 4-months old.¹³ Transgene expression was examined through development and ACSL1 protein was undetectable by Western blot in both wild-type (WT) and ACStg mice at birth (P0) despite ACSL1 mRNA expression being 13-fold greater in ACStg neonates compared to WT neonates (Fig. 1A, 1B). Increased ACSL1 protein in ACStg hearts was observed after P7 (Fig. 1A). Palmitate biodistribution measured by *in vivo* positron emission tomography (PET) at 12 weeks of age was increased 2-fold, indicating increased cardiac FA uptake in ACStg hearts

(Fig. 1C). At this time point, there was no increase of myocardial triglyceride content in ACStg hearts under random fed conditions (Fig. 1D). However, myocardial ceramide and diacylglycerol (DAG) content were significantly increased in ACStg hearts (Fig. 1E, 1F). Consistent with the previous report, this moderate increase of lipid uptake induced a modest increase in ventricular weight to body weight ratio and ventricular wall thickness (IVS) on the basis of cardiomyocyte hypertrophy in ACStg hearts (Fig. 1G-I, Supplemental Fig. I).¹³ Although there was no statistically discernable difference in LV end-diastolic volume (LVEDV) and LV ejection fraction (LVEF) measured by echocardiography (Fig. 1J, K), cardiac catheterization revealed a significant reduction in arterial blood pressure in ACStg mice accompanied by decreased max dP/dt and min dP/dt by the age of 24 weeks (Fig. 1L-N). Furthermore, BNP and alpha skeletal muscle actin (Acta1) expression were modestly increased in ACStg hearts by 2-fold (BNP) and 1.3-fold (Acta1) at the age of 12 weeks (Fig. 1O). Taken together, a 2-fold increase of lipid uptake induces modest cardiac hypertrophy with preserved systolic function at the age of 12 weeks, but impairs systolic function at the age of 24 weeks.

Figure 1: ACStg mice develop mild LVH with modest systolic dysfunction. (A) Representative western blot of Acsl1 protein expression in wild-type (WT) and Acsl1 transgenic mice (ACStg) from birth to 12-weeks of age. Numbers beneath each lane represents ACSL1 densitometry. The antibody recognizes both endogenous ACSL1 and the transgene. (B) mRNA expression of Acsl1 was quantified by RT-PCR at the age of P0 and 12-weeks. * $P < 0.05$, ** $P < 0.01$ vs. WT. (C) Representative PET image and quantification of $1\text{-}^{11}\text{C}$ palmitate biodistribution in 12-wk-old WT and ACStg hearts; $n = 10\text{-}12$. * $P < 0.05$ (D-F) Cardiac triacylglycerol (D), ceramide (E), or diacylglycerol (F) content in 12-week-old WT and ACStg hearts; $n = 5$. * $P < 0.05$ vs. WT. (G) Quantification of ventricular weight (VW) vs body weight (BW) ratio. $n = 4$ in each group. (H) Myocyte cross-sectional areas estimated from WGA-stained cross sections obtained from 24-wk-old ACStg mice and age-matched controls ($n = 2$ hearts per genotype). See Supplemental Fig. I for representative image. (I-K) Echocardiographic analysis. Interventricular septal thickness (I), Left ventricle end-diastolic volume (LVEDV) (J), LV ejection fraction (LVEF) (K), at 12 and 24-weeks of age. $n = 5$ at 12-weeks of age and $n = 4$ at 24-weeks of age. (L-M) Cardiac catheterization. Max dP/dt (L) and Min dP/dt (M) and arterial blood pressure (N) in ACStg hearts at 12 and 24-weeks of age. $n = 5$ at 12-weeks of age and $n = 4$ at 24-weeks of age. (O) BNP and Acta1 mRNA expression were quantified by RT-PCR at 12-weeks of age. $n = 4$, ** $P < 0.01$. All data are mean \pm sem.

Figure 2



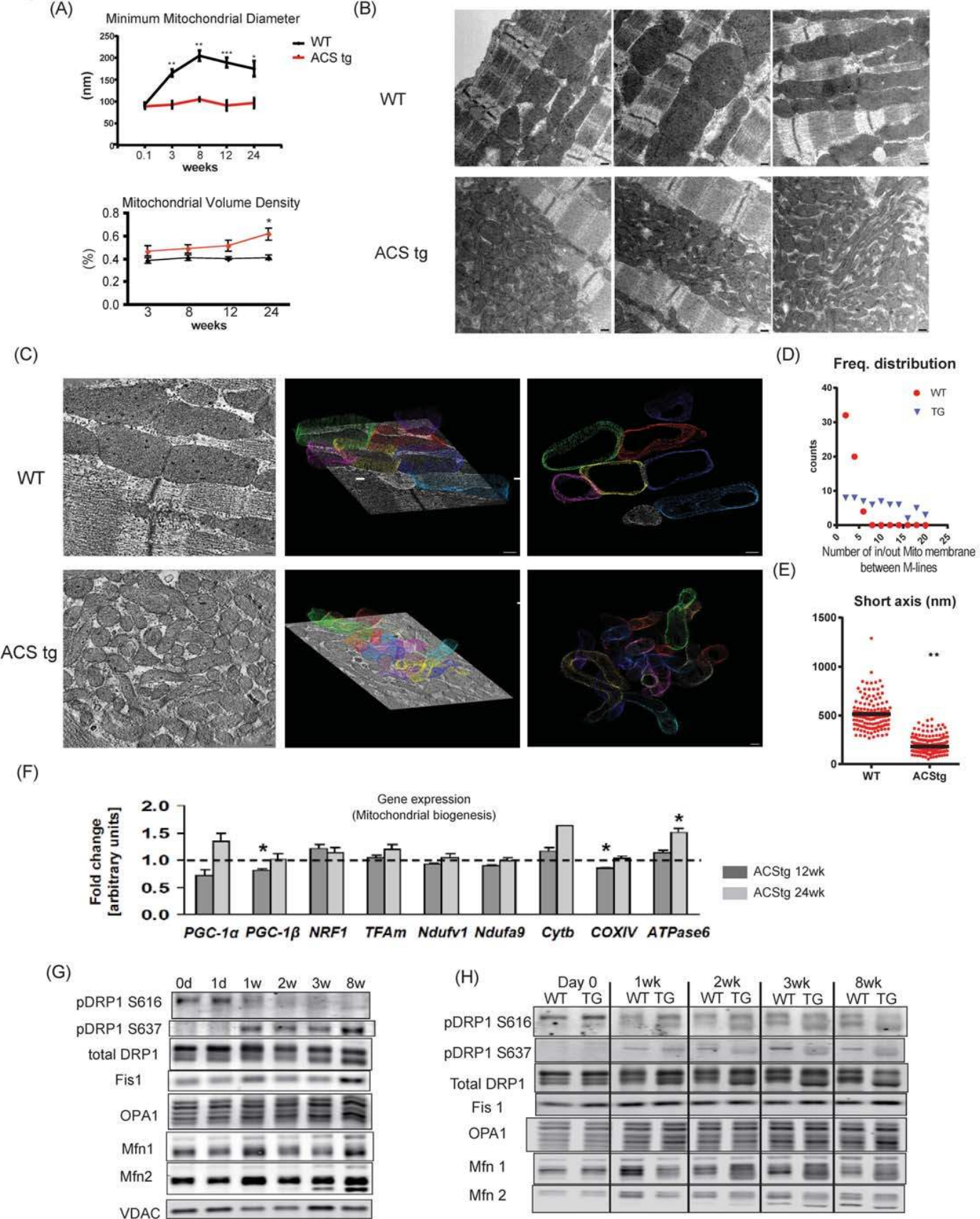
Increased respiration and ROS production in isolated mitochondria from ACStg hearts.

In ACStg mice, oxygen consumption rates and ATP synthesis rates in isolated mitochondria incubated with palmitoyl-carnitine as a substrate, were increased at 12-weeks of age, but were unchanged at 24-weeks of age relative to WT controls (Fig. 2A, 2B). In contrast, oxygen consumption rates were not impaired with pyruvate or glutamate as substrates at 12- and 24-weeks of age respectively (Fig. 2C, 2D). In addition, in-gel activities (in blue-native PAGE) of oxidative phosphorylation (OXPHOS) complexes I and IV were unchanged but complex V activity was increased at 12-weeks of age in ACStg hearts (Fig. 2E-G). Mitochondrial superoxide production (measured as H_2O_2 release from mitochondria) was increased 2-fold in ACStg heart mitochondria exposed to succinate or palmitoyl-carnitine as a substrate, and was completely inhibited by addition

of rotenone (Fig. 2H). Increased ROS was not observed when glutamate was used as a substrate (Supplemental Fig. II-A), suggesting that ROS production derives from reducing equivalents that are oxidized by complex II. Oxidation of 2',7'-dichlorofluorescein-diacetate (DCFDA) was increased in whole cell extracts of ACStg hearts (Fig. 2I). Moreover, increased mitochondrial 4-hydroxy-2-nonenal (4HNE) adducts in ACStg mitochondrial proteins, a highly toxic aldehyde byproduct of lipid peroxidation caused by ROS production, also supports increased mitochondrial ROS production (Fig. 2J). However, activity of mitochondrial aconitase was not reduced, suggesting that there was no increase in oxidative stress in the mitochondrial matrix of ACStg hearts, potentially the result of increased SOD2 content (Fig. 2K, Supplemental Fig. II-B). Thus, short-term low-level lipid overload does not initially impair mitochondrial oxidative capacity in the murine heart despite increasing ROS generation.

Figure 2: Mitochondrial respiratory function and ROS production in isolated mitochondria from ACStg hearts. (A,B) Maximal ADP-stimulated mitochondrial oxygen consumption (A) and ATP synthesis rates (B) in mitochondria isolated from 12- and 24-week-old WT and ACStg hearts using palmitoylcarnitine as a substrate; n =4-5. * P<0.05 vs. WT. (C,D) Maximal ADP-stimulated mitochondrial oxygen consumption in saponin-permeabilized cardiac fibers of 12- and 24-week-old WT and ACStg hearts using pyruvate (C) or glutamate (D) as a substrate; n =6. (E-G) Electrophoretic separation of OXPHOS complexes by blue-native PAGE (E), representative images of in-gel activities of complexes I, IV, and V (F), and quantification of OXPHOS complex activities (G), measured in 12-week-old WT and ACStg hearts; n =4. *P<0.05 vs. WT. (H) H_2O_2 production with succinate as a substrate in mitochondria isolated from 12- or 24- week-old WT and ACStg hearts, or with palmitoyl-carnitine as a substrate in mitochondria from 12-week-old WT and ACStg hearts, in the absence or presence of rotenone (Rot); n =3 at 12wks, n =6 at 24wks. *P<0.05 vs. WT. (I) Oxidation of DCFDA in whole tissue extracts of 24-week-old WT and ACStg hearts; n =5-6. *P<0.05 vs. WT. (J) Western blot for 4HNE protein adducts in mitochondrial protein isolated from WT and ACStg hearts. Numbers beneath each lane represent densitometry of 4HNE immunoreactivity of all bands in that lane. (K) Aconitase activity measured in mitochondria isolated from 12- or 24-week-old WT and ACStg hearts; n =3 at 12weeks, n =6 at 24weeks. All data are mean \pm sem.

Figure 3



Postnatal increase in mitochondrial cross-sectional area is attenuated in lipid-overloaded cardiomyocytes.

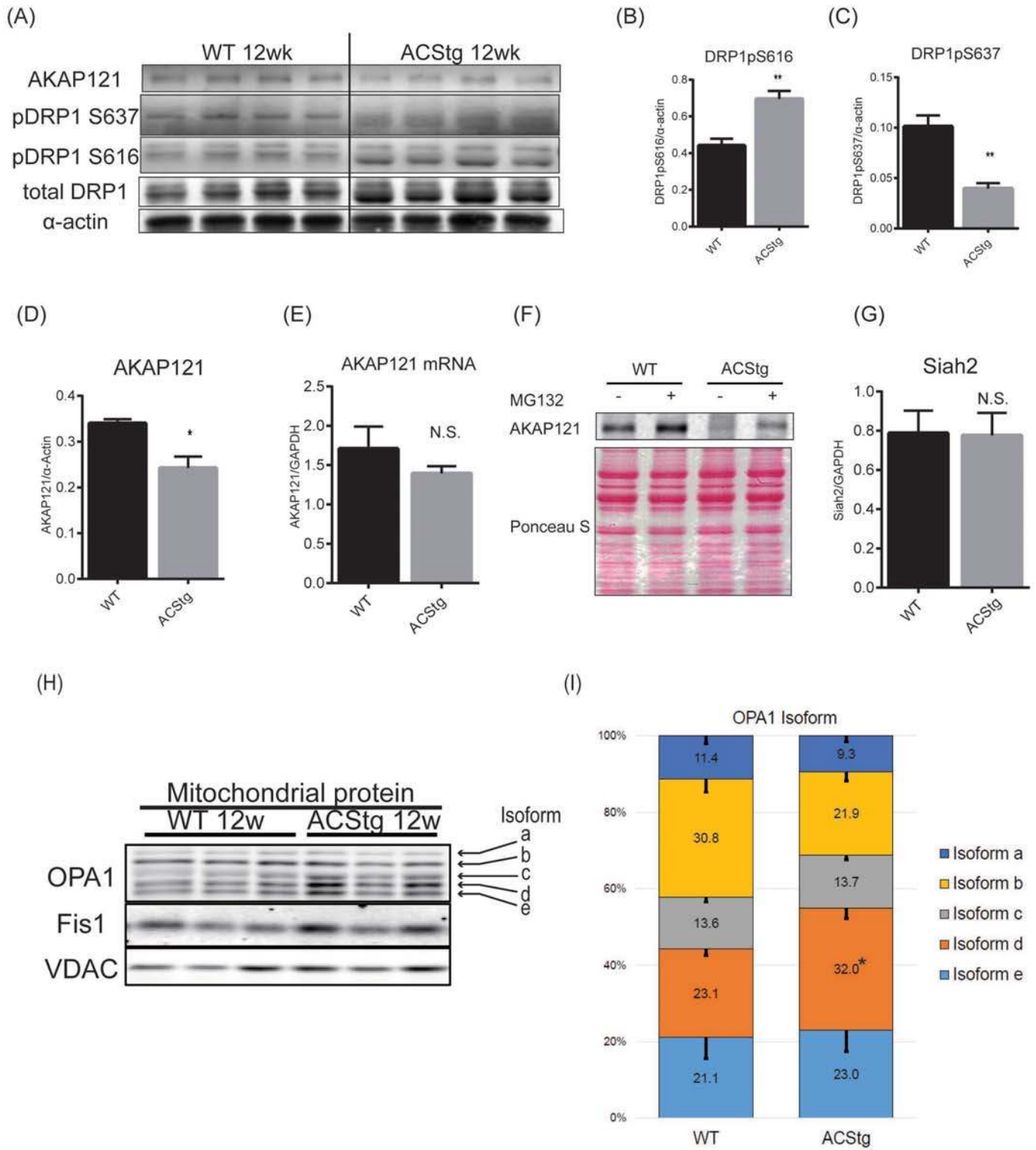
We next investigated mitochondrial morphology. During the early postnatal period, cardiomyocytes dynamically change their structure and function to adapt to the increased workload and oxygen consumption that parallels the switch of substrate utilization from glycolysis to mitochondrial fatty acid oxidation.³ Mitochondrial morphology also changes and volume density increases as they become larger and more ovoid in shape.¹⁴ 2-D Electron microscopy revealed that mitochondrial dimension in WT hearts increased 2-fold within the first 3 weeks after birth before plateauing (Fig. 3A, Supplemental Fig. III-A). This postnatal mitochondrial enlargement was absent in ACStg mice (Fig. 3A, Supplemental Fig. IIIA). In contrast, mitochondrial volume density was significantly increased in ACStg hearts (Fig. 3A, 3B, Supplemental Fig. III-B, III-C), based upon the appearance of accumulated small mitochondria. To evaluate mitochondrial morphology more precisely, we performed 3D-transmission electron microscopic tomography at the age of 8 weeks. 3D mitochondrial images revealed the presence of narrow but elongated mitochondria whose tortuous shapes crossed individual sectioning planes more than once (Fig. 3B, 3C). This is associated with an increase in number of cytosol-mitochondrial membrane transitions on any projection between the Mlines of neighboring myofilament bundles (Fig. 3D) The short axis diameter of mitochondria was significantly reduced in ACStg hearts by 60% (Fig. 3E). Taken together, perinatal lipid overload significantly alters age-dependent structural mitochondrial remodeling, characterized by a reduction in minimum diameter and morphological changes that are consistent with fragmentation of the mitochondrial network.

These morphological changes could also reflect increased biogenesis or altered dynamics of the mitochondrial network. To address this, we examined mRNA expression levels of peroxisome proliferator-activated receptor γ co-activators 1 α/β (PGC-1 α/β) and their targets, but found no evidence for increased mitochondrial biogenesis signaling (Fig. 3F). Thus, we hypothesized that lipid overload may alter signaling pathways that regulate mitochondrial dynamics.

Mitochondrial dynamics is regulated by the activity of the dynamin superfamily of large GTPases, specifically mitofusin 1 and 2 (Mfn1 and Mfn2), optic atrophy 1 (Opa1), and dynamin related protein 1 (DRP1).^{15,16} Mitochondrial fusion is mediated by OPA1 and Mfn1/2 which reside on mitochondrial inner and outer membranes respectively. Fission is controlled by the cytosolic protein DRP1 that translocates from the cytosol to mitochondrial membranes following post-translational modifications to interact with the outer mitochondrial membrane protein Fis1. We determined the protein levels of these mitochondrial fusion and fission proteins and DRP1 phosphorylation during postnatal cardiac growth. Western blot analysis of whole heart lysates from wild-type mice revealed that DRP1 phosphorylation dramatically changed during the first 3 weeks of life (Fig. 3G, Supplemental Fig. IV-A). Consistent with increased postnatal mitochondrial dimensions (fusion), DRP1 phosphorylation at S616, which activates DRP1-mediated mitochondrial fission, declined with age. In contrast, DRP1 phosphorylation at S637, which induces mitochondrial fusion by inhibiting DRP1-mediated mitochondrial fission, increased over time (Fig. 3G, Supplemental Fig. IV-A). This developmental increase in DRP1 S637 phosphorylation was not observed in ACStg mice (Fig. 3H, Supplemental Fig. IV-B). These data suggest that cardiac lipid overload impairs postnatal mitochondrial remodeling by modulating DRP1 phosphorylation.

Figure 3: Mitochondrial fragmentation in ACStg hearts. (A) Postnatal mitochondrial enlargement was attenuated in ACStg hearts. Stereologic quantification of mitochondrial minimum diameter and volume density was performed at the ages as indicated in 2-D electron micrographs (EM) presented in Supplemental Fig. III-A. ; n =3-4. * P<0.05, ** P<0.01, *** P<0.001. (B) Representative electron micrographs of longitudinal sections of WT and ACStg cardiomyocytes at the age of 8weeks, 3 hearts per genotype. Scale bars indicate 200nM. (C-E) Representative electron tomographic micrographs and corresponding 3D models of the mitochondrial network. Scale bars indicate 100nM (C). Number of mitochondrial outer membranes transitioned on a straight line trajectory between M-lines of two neighbouring myofilament bundles, counted in 22 (WT) and 26 (ACStg) electron tomograms (3 hearts per genotype) (D). Short axis diameter was measured in 132 (WT) and 290 (ACStg) mitochondria of 22 (WT) and 26 (ACStg) electron tomograms from 3 hearts per genotype; ** P <0.01(E). (F) Myocardial gene expression in 12- and 24-week-old WT and ACStg mice normalized to 16S RNA transcript levels. Values represent fold change in mRNA transcript levels relative to WT, which was assigned as 1 (dashed line), n=8 *; P<0.05 vs WT. (G) Western blot of whole heart lysates probed with antibodies as indicated at postnatal ages as shown. d=day, w=week. See also Supplemental Fig. IV-A. Each sample at 0d, 1w and 3w was isolated more than 3 times and immunoblotted separately, and each sample at day1, 2w and 8w was repeated twice. A representative western blot is shown. (H) Western blot of whole heart lysates from WT and ACStg mice probed with antibodies as indicated and harvested at the ages shown. See also Supplemental Fig. IV B. All data are mean \pm sem. Each sample at day0, 1wk and 3wk was isolated more than 3times and immunoblotted separately, and each sample at 2wk and 8wk was repeated twice. A representative western blot is shown.

Figure 4



Lipid overload alters ubiquitin-proteasome mediated AKAP121 degradation and OPA1 proteolysis.

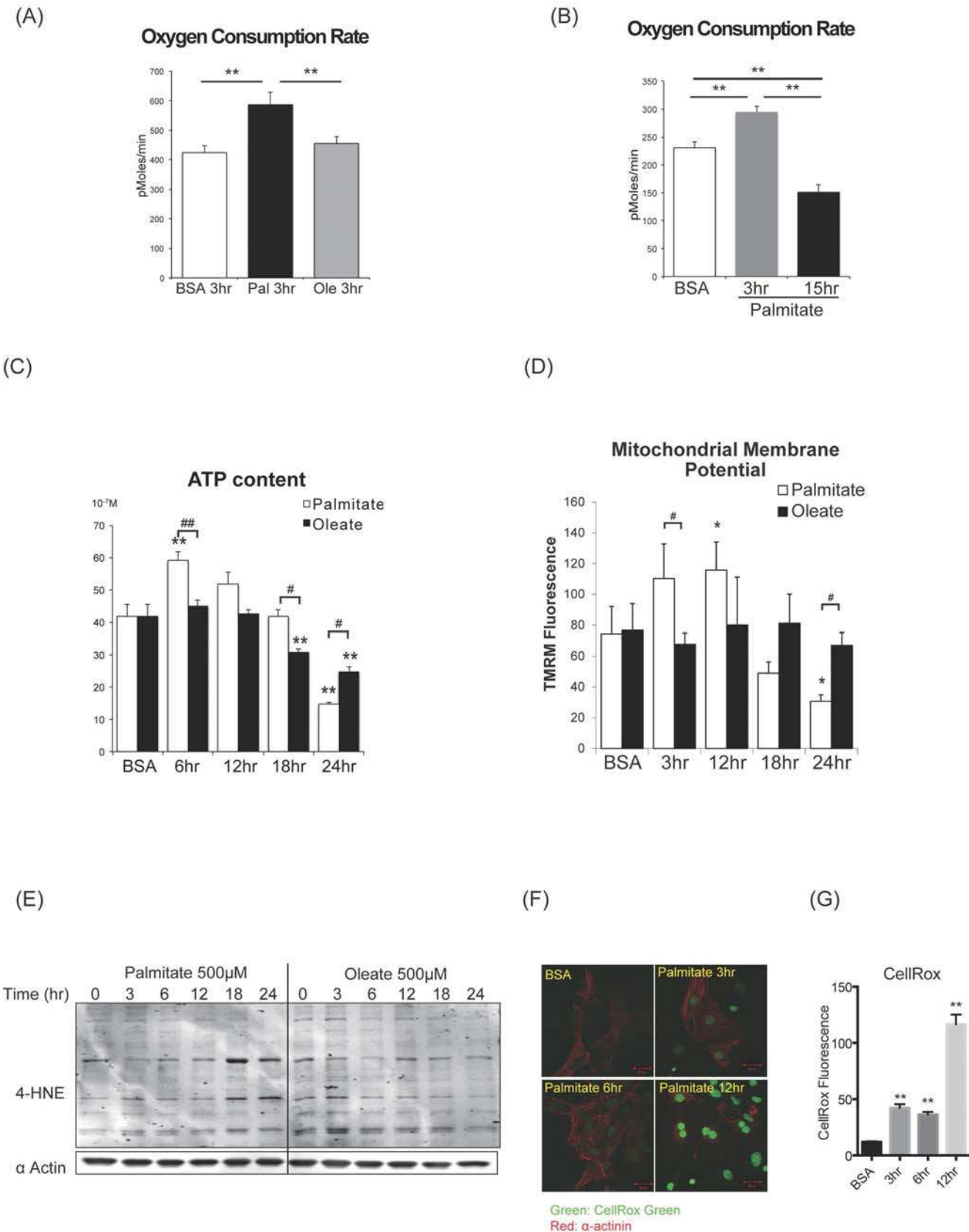
Protein kinase A (PKA) mediated DRP1 phosphorylation at S637 inhibits DRP1 localization to mitochondria and subsequent mitochondrial fission.¹⁷ The mitochondrial localization of PKA and its ability to phosphorylate DRP1 is mediated by ubiquitin-proteasome mediated degradation of A kinase anchoring protein 121 (AKAP121), which are mitochondrial outer membrane scaffold proteins.¹⁸⁻²⁰ We therefore examined whether AKAP121 protein content might be decreased in ACStg hearts. In 12-week-old ACStg mouse hearts, western blotting revealed that DRP1 phosphorylation at S637 was significantly reduced and phosphorylation at S616 increased (Fig. 4A-C). In addition, AKAP121 expression was also significantly decreased in ACStg hearts relative to WT (Fig. 4A, 4D), which was not related to any difference in AKAP121 mRNA expression (Fig. 4E). Therefore we tested whether posttranslational regulation by the ubiquitin-proteasome system (UPS) might increase AKAP121 degradation in the face of lipid overload. WT or ACStg mice were injected intraperitoneally with MG132 or DMSO and whole heart homogenates were subjected to western blot analysis. The proteasome inhibitor MG132 blocked the reduction of AKAP121

protein content in ACStg mice, suggesting that AKAP121 is degraded by the UPS pathway in response to lipid overload (Fig. 4F). AKAP121 is a target of the ubiquitin ligase Siah2 in the context of hypoxia.²⁰ However, Siah2 mRNA expression was not increased in ACStg hearts (Fig. 4G). Taken together, lipid overload altered DRP1 phosphorylation by enhancing AKAP121 degradation which may be independent of the hypoxia-stimulated pathway.

We also examined whether the mitochondrial fusion protein, OPA1, could be affected by lipid overload. There are at least 8 mRNA variants of OPA1 as a result of alternative splicing.²¹ Variants 1 and 7 are dominant variants in mammalian cells. In response to decreased mitochondrial membrane potential, OPA1 also undergoes proteolytic cleavage which impairs its ability to induce mitochondrial fusion.²² Western blot analysis of heart mitochondrial protein showed 5 bands of OPA1; 2 fusion-competent long-isoforms and the 3 fusion-incompetent short-isoforms generated by the proteolytic processing of the 2 long-isoforms (Fig. 4H). Consistent with enhanced mitochondrial network fragmentation in ACStg hearts, the ratio of short-form to long-form was increased by 1.7-fold in ACStg hearts (Fig. 4H, 4I). Thus, these data support the hypothesis that mitochondrial dynamics shifts towards enhanced mitochondrial fission by at least two distinct mechanisms.

Figure 4: Differential post-translational modifications of DRP1 and OPA1 in ACStg mice. (A-D) Decreased protein content of AKAP121, and altered phosphorylation profile of DRP1. Whole heart lysates were subjected to western blot analysis (A) and densitometric quantification of DRP1pS616 (B), DRP1pS637 (C) and AKAP121 (D), n = 4. ** P < 0.01, * P < 0.05. (E) AKAP121 mRNA expression of 12-week-old WT and ACStg mice was determined by quantitative RT-PCR (n=4) (F) AKAP121 degradation is mediated by the Ubiquitin-Proteasome pathway in ACStg hearts. WT or ACStg mice were injected intraperitoneally twice with DMSO or MG132 (18hrs and 6hrs before euthanasia). Whole-heart lysates were subjected to western blot analysis. (G) Siah2 gene expression in 12-week-old WT and ACStg mouse hearts was determined by realtime-PCR. Values are normalized to GAPDH expression. n=4. (H & I) Increased OPA1 cleavage in ACStg hearts. Mitochondrial fractions were prepared from 12-week-old WT or ACStg hearts and subjected to western blot analysis. Each lane shows the sample from different animals. The top 2 bands correspond to non-cleaved isoforms of OPA1 (long-form) and the bottom 3 bands correspond to cleaved isoforms of OPA1 (short-form) (H), quantitative densitometric analysis of OPA1 isoforms (I), n = 4. * P < 0.05 vs. WT. All data are mean ± sem.

Figure 5



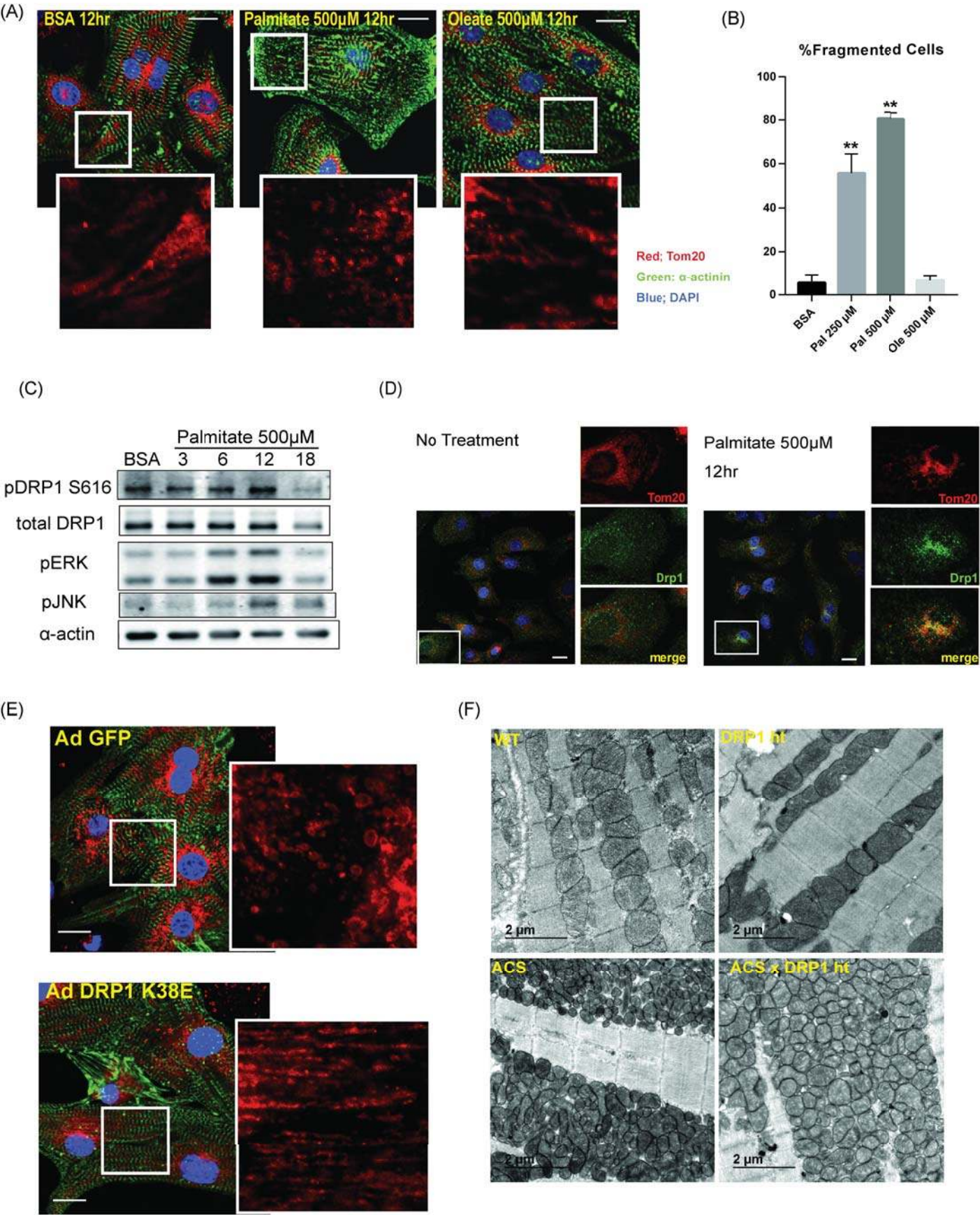
Effect of long chain FA, palmitate and oleate on mitochondrial respiration and ROS production in rat neonatal cardiomyocytes.

To more directly determine the mechanistic basis for the mitochondrial adaptation to lipid overload, we treated cultured rat neonatal cardiomyocytes (NRVCs) with free fatty acids (FFAs). Because saturated fatty acids are the main mediators of lipotoxicity,^{23, 24} we treated NRVCs with bovine serum albumin (BSA)-conjugated palmitic acid (C16:0) to mimic lipid overload *in vivo*, and compared them with cells treated with the non-saturated fatty acid, oleic acid (C18:1). Oxygen consumption of lipid-treated NRVCs was determined with the Seahorse XF24 flux analyzer. Although short exposure to palmitate (<4h) increased mitochondrial oxygen consumption rates (OCR) in NRVCs, continued exposure (>8h) reduced OCR (Fig. 5A, 5B, Supplemental Fig. V-A, V-B). In contrast, oleate treatment did not alter mitochondrial OCR (Fig. 5A). To

confirm that this increase of OCR is coupled to mitochondrial oxidative phosphorylation and ATP synthesis, we examined time course changes of mitochondrial membrane potential and ATP content after palmitate treatment. Consistent with OCR, palmitate treatment initially increased mitochondrial membrane potential and ATP content, but these parameters declined after continued incubation for more than 12h (Fig. 5C, 5D). We also examined ROS production of cardiomyocytes after palmitate or oleate treatment. As expected, western blotting of 4HNE revealed that ROS production was increased after palmitate treatment (Fig. 5E). CellROX Green (ROS probe) also accumulated in the nucleus after 12hrs of palmitate treatment (Fig. 5F, 5G). In contrast, oleate treatment did not increase 4HNE accumulation (Fig. 5E). Taken together, palmitate supplementation initially accelerates mitochondrial respiration that is coupled to ATP synthesis. However, continued exposure to palmitate induces mitochondrial respiratory failure, potentially on the basis of ROS-induced injury.

Figure 5: Mitochondrial metabolism and ROS production in rat neonatal cardiomyocytes following increasing duration of free fatty acids exposure. (A) Basal oxygen consumption rate (OCR) (assayed by the Seahorse XF24 system) in NRVCs incubated with BSA alone, palmitate-BSA (500μM) or oleate-BSA (500μM). ** P<0.01. **(B)** Time course analysis of OCR of NRVCs treated with palmitate-BSA. Increased basal OCR after short-term exposure to palmitate (3hr) and reduced basal OCR after long-term exposure (15hr) of palmitate. **P <0.01 . See also Supplemental Fig. V. **(C)** Time course analysis of ATP content in NRVCs after palmitate or oleate treatment. ** P<0.01 vs BSA # P<0.05, ## P<0.01. **(D)** Time course analysis of mitochondrial membrane potential after palmitate or oleate treatment. Cardiomyocytes were stained with TMRM and Hoechst at indicated times and fluorescence intensity was assayed with a plate reader. The ratio of TMRM/Hoechst fluorescence are shown. n = 4, * P<0.05 vs BSA, # P<0.05. **(E)** Western blot for 4HNE protein adducts in NRVCs after palmitate or oleate treatment. **(F & G)** CellROX green staining in NRVCs after palmitate treatment. CellROX Green is a DNA dye, and upon oxidation, it binds to DNA. Representative confocal image (F) and fluorescence intensity was quantified (G). ** P<0.01 vs BSA. All data are mean±sem. Scale bars indicate 20μm.

Figure 6



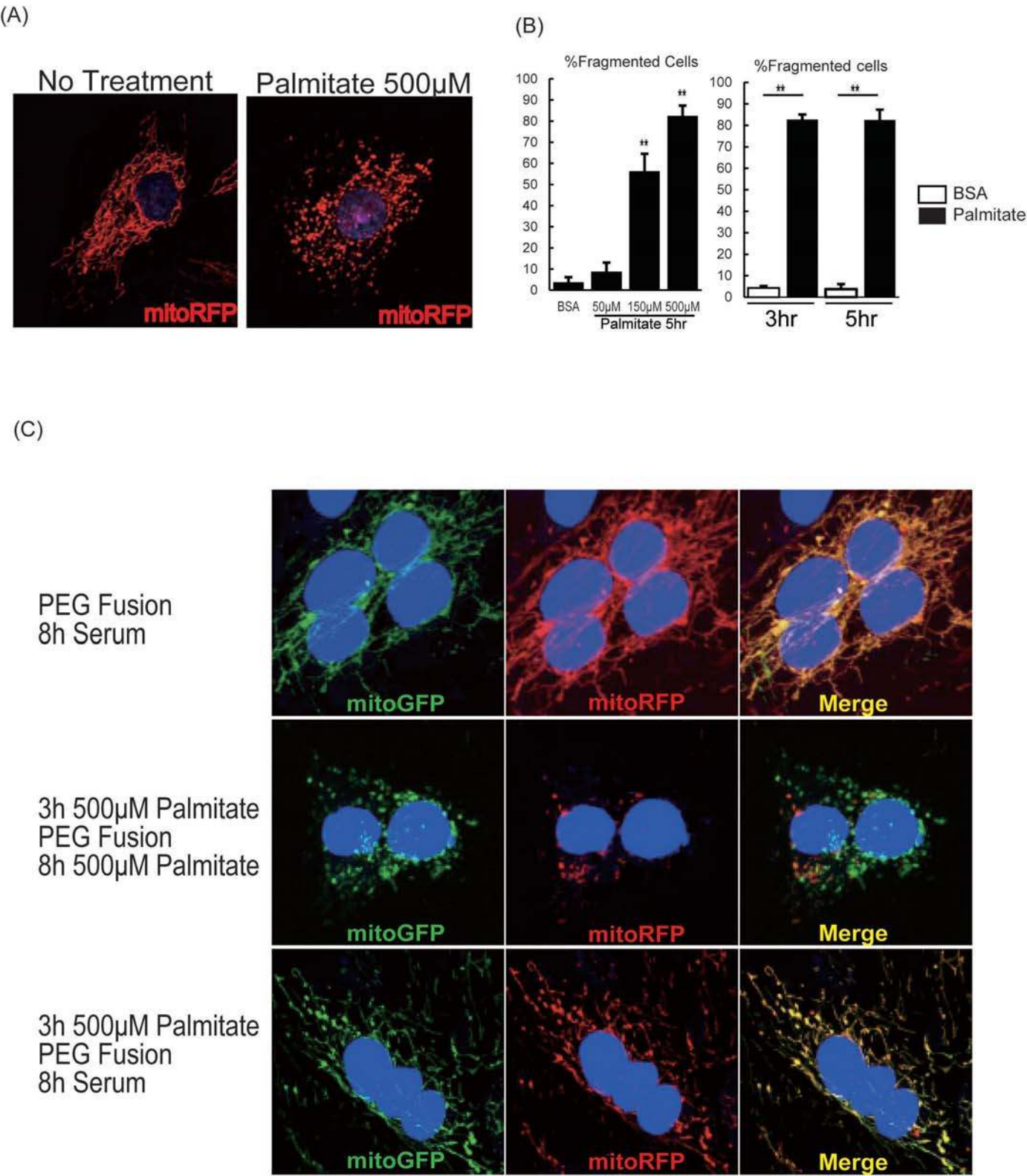
Altered mitochondrial dynamics in response to lipid overload is mediated in part by post-translational modification of DRP1.

We next determined if mitochondrial dynamics is modulated by fatty acids in NRVCs. To visualize the mitochondrial network, cardiomyocytes were stained with mitotracker in live cells or immunostained with an anti-Tom20 antibody in fixed cells. The normal mitochondrial network in NRVCs appeared as tubular mitochondria (Fig. 6A, Supplemental Fig. VI-A). Palmitate supplementation changed mitochondrial morphology from a tubular to small rounded shape (Fig. 6A, 6B, Supplemental Fig. VI-A). Interestingly, these morphological changes were not observed in oleate-treated cardiomyocytes (Fig. 6A, 6B). We examined DRP1 phosphorylation profiles in NRVCs after palmitate treatment. Similar to P0 hearts (Fig. 3G, 3H), we

detected no phosphorylation at S637 in isolated NRVCs throughout the time course. Instead, palmitate treatment increased DRP1 phosphorylation at S616 in NRVCs (Fig. 6C). Immunohistochemistry revealed DRP1 translocation from the cytosol to mitochondria in response to palmitate treatment (Fig. 6D). To validate that DRP1 mediates mitochondrial network fragmentation in lipid overload, we examined the effect of DRP1K38E, a dominant negative mutant of DRP1.²⁵ DRP1K38E overexpression prevented palmitate-induced mitochondrial network fragmentation in NRVCs (Fig. 6E, Supplemental Fig. VII A). Furthermore, the reduced mitochondrial cross-section area observed was partially reversed in ACStg mice that lacked one *DRP1* allele in cardiomyocytes (ACStg *DRP1*^{+/-}) (Fig. 6F, Supplemental Fig. VII B-E). Taken together, palmitate exposure shifts mitochondrial dynamics towards fission and away from fusion, in part via a DRP1-mediated mechanism.

Figure 6: DRP1 mediates mitochondrial fission after lipid overload. (A) Rat neonatal cardiomyocytes were stimulated with growth medium with or without 500μM palmitate or oleate. 12hrs after stimulation, cells were fixed with 4% paraformaldehyde and immunostained with α-actinin (green), Tom20 (red) and DAPI (blue). Scale bars indicate 20μm. (B) Quantification of mitochondrial fragmentation presented in Figure 6A. More than 100 cells were counted to determine the percentage (%) of cells with fragmented mitochondria. n=3, **: P<0.01. (C) Increased phosphorylation of DRP1 at Ser616 after palmitate treatment. NRVCs were treated in growth medium with 500μM palmitate and cell lysates were harvested at the indicated times in hr. (D) NRVCs were treated in growth medium with or without 500μM palmitate and subjected to immunohistochemistry for DRP1 (green) and Tom20 (red). Note that DRP1 is co-localized with Tom20 after palmitate treatment. Scale bars indicate 20μm. (E) NRVCs were infected with AdGFP or Ad DRP1K38E and were treated in growth medium with 500μM palmitate. NRVCs were subjected to immunohistochemistry for α-actinin (green) and Tom20 (red). See also Supplemental Fig. VII-A. Scale bars indicate 20μm. (F) Representative electron micrographs of longitudinal heart sections obtained from WT, *DRP1*^{+/-}, ACStg, and ACStg × *DRP1*^{+/-}. DRP1 knockdown partially rescued mitochondrial morphology in ACStg hearts. See also Supplemental Fig. VII B-E.

Figure 7

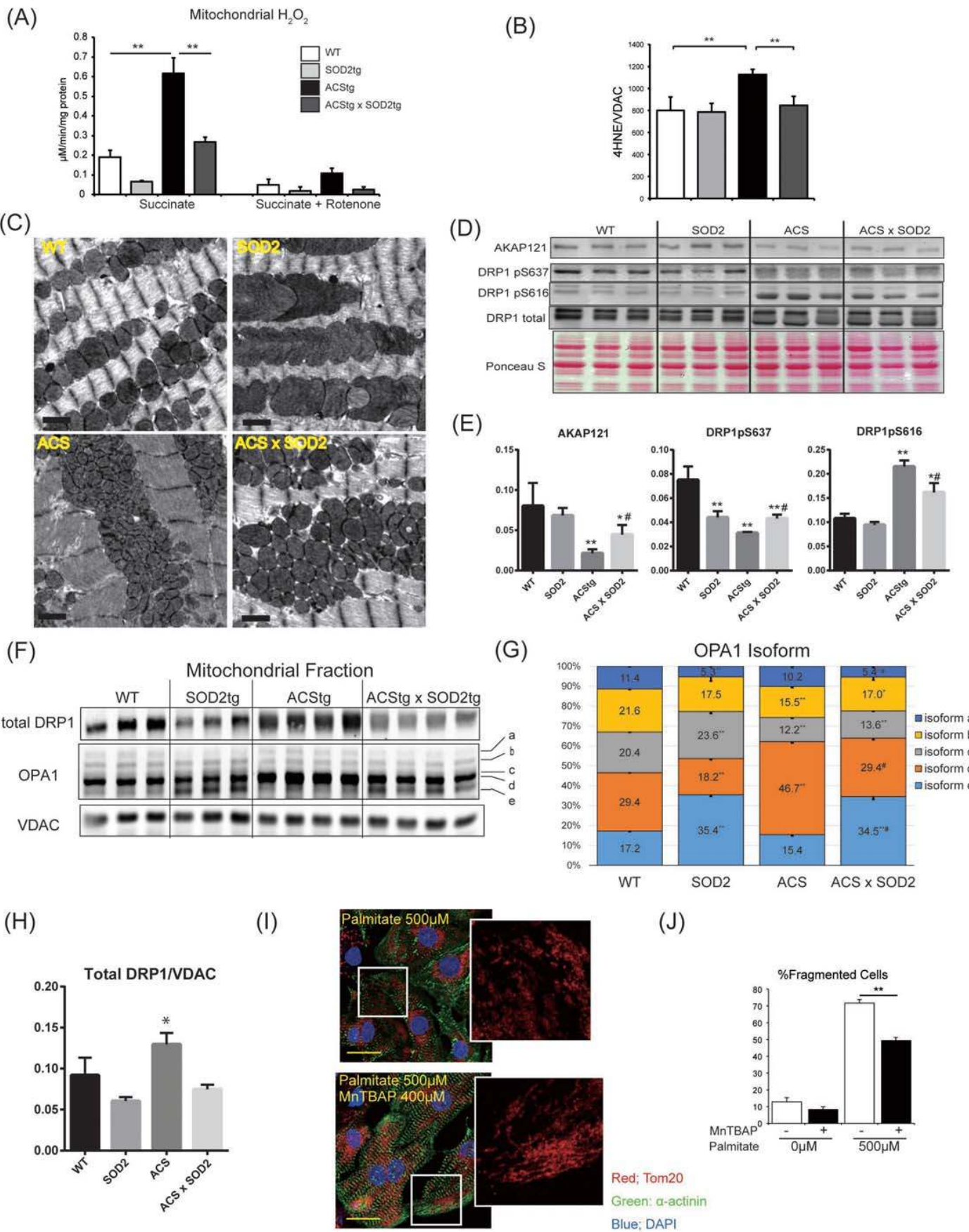


Mitochondrial morphology reflects the balance of mitochondrial fusion and fission. To directly evaluate if palmitate exposure inhibits mitochondrial fusion leading to mitochondrial network fragmentation, we co-cultured L6 myoblasts expressing either mitoGFP or mitoRFP and induced cell fusion with polyethylene glycol (PEG). L6 myoblasts displayed mitochondrial network fragmentation which was evident after 3hrs of palmitate supplementation (Fig. 7A, 7B). Mitochondrial network fragmentation was further augmented when expression of ACSL1 was increased following retroviral transduction (Supplemental Fig. VI-B). After the induction of cell fusion with PEG, fusion of GFP and RFP-labeled mitochondria was evident in cells treated with control media when imaged 8hr

following PEG-induced cell fusion (Fig. 7C top). In contrast, mitochondrial fusion was not observed in the cells incubated with palmitate-supplemented medium (Fig. 7C middle). To determine if palmitate pre-exposure permanently impacted mitochondrial fusion in L6 myoblasts, cells were pretreated with palmitate supplemented medium for 3hr that disrupted the mitochondrial network and then the medium was replaced with normal growth medium. Mitochondria regained their tubular structure following removal of palmitate, and fusion of GFP and RFP mitochondrial populations was observed, suggesting that palmitate-induced defects in mitochondrial fusion are reversible (Fig. 7C bottom).

Figure 7: Mitochondrial fusion in L6 myoblasts was impaired by palmitate exposure. (A) L6 myoblasts transfected with mitoRFP were incubated in growth medium with or without 500 μ M palmitate for 5h, and representative images are shown. (B) Cells were evaluated to quantify tubular or fragmented mitochondrial networks, and cells with fragmented mitochondria were expressed as percentage of all viewed cells, n=4 and 80 cells counted per group. ** $P < 0.01$ vs BSA. All data are mean \pm sem. (C) L6 myoblasts were transfected either with mitoRFP or mitoGFP, co-plated (25,000 cells each) on cover slips for 24h, and then cell fusion was induced with polyethylene glycol (PEG). Cells were fused for 8h in regular growth medium with no palmitate (top row), 8h in growth medium with 500 μ M palmitate, following 3h pre-incubation with 500 μ M palmitate prior to PEG fusion (middle row), or 8h in the regular growth medium with no palmitate, following 3h pre-incubation with 500 μ M palmitate prior to PEG fusion (bottom row).

Figure 8



Contribution of mitochondrial ROS generation to FA-mediated mitochondrial fragmentation.

In light of our observations of increased lipid-mediated ROS production *in vivo* and *in vitro* that correlated with mitochondrial network fragmentation, we tested the hypothesis that elevated mitochondrial ROS production may initiate downstream signaling events to alter mitochondrial dynamics. Because mitochondrial superoxide dismutase 2 (SOD2) mediates superoxide detoxification at a diffusion limiting rate in the mitochondrial matrix,²⁶ we examined whether SOD2 overexpression could rescue altered mitochondrial morphology in ACStg hearts. We generated a cardiac-specific double-transgenic mouse harboring SOD2 and ACSL1 transgenes (ACS × SOD2 mice). As expected, enhanced superoxide production and increased 4HNE adducts observed in ACStg mitochondria were almost completely rescued by the overexpression of SOD2 (Fig. 8A, 8B, Supplemental Fig. VIII-A). Mitochondrial cross-sectional area and apparent number were normalized in ACStg hearts by SOD2 overexpression (Fig. 8C, Supplemental Fig. VIII-B). Surprisingly, SOD2 overexpressing cardiomyocytes with reduced ROS production, demonstrated a 4-fold increase in mitochondrial cross-sectional

area estimated from 2-D images, suggesting that mitochondrial ROS levels are inversely correlated with mitochondrial dimensions (Fig. 8A, 8C).

Finally, we determined if altered DRP1 phosphorylation or changes in OPA1 processing in ACStg mice were prevented by SOD2 overexpression. Western blot analysis showed that protein expression of AKAP121 and DRP1 phosphorylation at S637 was increased and DRP1 phosphorylation at S616 was reduced by SOD2 overexpression (Fig. 8D, 8E). In addition, total levels of DRP1 normalized to VDAC, which were increased in ACStg hearts, were normalized by SOD2 overexpression (Fig. 8F, 8H). Overexpression of ACSL1 enhanced OPA1 proteolysis to specifically increase short isoform-d formation (Fig. 8F, 8G). Relative to ACStg, in SOD2/ACS double transgenic mice there was a reduction in isoform-d and an increase in isoform-e (Fig. 8F, 8G). *In vitro*, MnTBAP, the SOD mimetic and peroxynitrite scavenger, partially normalized palmitate-induced mitochondrial network fragmentation in NRVCs (Fig. 8I, 8J). Taken together, these data indicate that mitochondrial redox signaling regulates mitochondrial dynamics by post-translational modulation of mitochondrial fusion and fission proteins.

Figure 8: Mitochondrial superoxide dismutase (SOD2) overexpression partially rescued abnormal mitochondrial dynamics in ACStg mice. (A,B) Enhanced ROS production in ACStg hearts was rescued by SOD2 overexpression. H₂O₂ production was determined in isolated mitochondria from 12-week-old WT, SOD2tg, ACStg and SOD2 × ACS double tg hearts in the absence or presence of rotenone **(A)**. Mitochondrial fractions were prepared from 12-week-old WT, SOD2tg, ACStg and SOD2 × ACS double transgenic hearts and subjected to western blot for 4HNE and quantified by densitometry **(B)**, n = 3–4 in each group. ** P < 0.01. See also Supplemental Fig. VIII-A **(C)** SOD2 overexpression partially rescued fragmented mitochondria in ACStg hearts. Representative electron micrographs from WT, SOD2tg, ACStg and SOD2 × ACS double tg mice. Bar indicates 1 μm. See also Supplemental Fig. VIII-B. **(D–H)** SOD2 overexpression reversed altered phosphorylation pattern of Drp1 and processing of OPA in ACStg hearts. Mitochondrial fractions were prepared from 12-week-old WT, SOD2tg, ACStg and SOD2 × ACS double tg hearts and subjected to western blot analysis for AKAP121 and total and phosphorylated Drp1 at Ser637 and Ser616 and the distribution of OPA1 isoforms were quantified **(F–H)**. n = 3–4 in each group. * P < 0.05, ** P < 0.01 vs WT, # P < 0.05 vs ACStg. **(I, J)** MnTBAP prevented palmitate-induced mitochondrial fragmentation in NRVCs. NRVCs were treated with or without 400 μM MnTBAP, a SOD mimetic and peroxynitrite scavenger, and then stimulated with or without growth medium containing 500 μM Palmitate. After 12h of stimulation, cells were fixed and stained with Tom20 antibody. Representative image from each group. **(I)** and quantification of the ratio of fragmented cells **(J)**, n = 3 in each group. ** P < 0.01. Scale bars indicate 20 μm.

Discussion

Recent studies have suggested that impaired mitochondrial energetics may contribute to the increased risk of heart failure in type-2 diabetes.⁸ The pathophysiology of mitochondrial dysfunction in diabetes is complex and may include altered insulin signaling, glucotoxicity and lipotoxicity. Prior work from our group suggested that impaired myocardial insulin signaling could precipitate mitochondrial dysfunction in the heart.¹¹ Given the likelihood that lipotoxicity could have distinct effects on mitochondria, the present study was designed to model increased myocardial lipid accumulation to a level that was similar in magnitude to that reported in animal models of obesity and diabetes.²⁷ We therefore utilized mice with cardiomyocyte-specific low-level overexpression of ACSL1, which gradually developed myocardial dysfunction and recapitulated key observations in neonatal cardiomyocytes that were incubated with palmitate. First, we observed that lipid overload initially enhances mitochondrial respiration coupled to ATP synthesis. However, prolonged lipid overload enhanced mitochondrial ROS generation, which is followed by reduced mitochondrial respiration and ATP synthesis. Second, we observed differential metabolic fates of palmitate and oleate in NRVCs. Our data indicates that increased mitochondrial respiration after palmitate supplementation results in accumulation of mitochondrial ROS and impaired mitochondrial energetics. Conversely, oleate supplementation did not increase mitochondrial respiration or ROS production and did not precipitate mitochondrial impairment. Third, mitochondrial redox status might influence mitochondrial morphology by modulating the post-translational modifications of proteins that regulate mitochondrial dynamics. Lipid overload increased AKAP121 ubiquitination, modulated DRP1 phosphorylation and altered OPA1 processing. Future studies in models with inducible increases in myocardial lipid uptake will be needed to determine if these mechanisms also alter mitochondrial dynamics and energetics in adult (postnatal) murine hearts. Prior studies from our laboratory showed altered mitochondrial morphology in db/db diabetic mice or type-1 diabetic Akita mice, which was accompanied by enhanced mitochondrial ROS production.^{10, 28} A recent study also revealed that right atrial cardiomyocytes isolated from type-2 diabetic patients exhibit increased mitochondrial ROS production and impaired mitochondrial bioenergetics.²⁹ Taken together, these observations suggest that the mechanism observed in the present study could be universally applicable to the pathophysiology of mitochondrial dysfunction in lipotoxic cardiomyopathy associated with obesity or diabetes mellitus.

Following uptake of FAs in cardiomyocytes, ACSLs immediately catalyze FAs to Acyl-CoA esters, which enter a variety of lipid metabolic pathways such as FA oxidation, TG synthesis/storage, phospholipid metabolism, and *de novo* ceramide synthesis. Cardiac ACSL1 over expression *in vivo* increases mitochondrial ROS production and the content of reactive lipid metabolites. We used a genetic approach to modulate mitochondrial ROS production by overexpressing ACSL1, SOD2, or both and demonstrated that mitochondrial redox status correlates with mitochondrial morphology. In addition, mitochondrial redox status is also associated with processing of mitochondrial proteins, such as OPA1 proteolysis, ubiquitin proteasome mediated degradation of AKAP121 and DRP1 phosphorylation at S637. DRP1 phosphorylation at S616, a target site for MAP kinases and CDK1,³⁰⁻³² also correlated with mitochondrial redox status and was recapitulated by *in vitro* palmitate treatment of NRVCs. These data are also supported by a recent publication showing that the ROS modulator 1 (ROMO1), a mitochondrial protein, is a redox-sensitive factor that regulates mitochondrial morphology by affecting OPA1 cleavage and oligomerization.³³

A recently described mechanism that may also induce mitochondrial fission is hypoxia. Siah2, a RING finger ubiquitin ligase induced by hypoxia, mediates ubiquitin-proteasome degradation of AKAP121. Subsequent reduction of PKA-dependent inhibitory phosphorylation of DRP1 is an important regulatory pathway for hypoxia induced mitochondrial fission.²⁰ In ACStg hearts, we also observed substantial proteasome mediated degradation of AKAP121 and mitochondrial redox status was correlated with AKAP121 protein levels and DRP1 phosphorylation at S637. However, in contrast to hypoxia, Siah2 mRNA induction was not observed in ACStg hearts (Fig. 4G), suggesting that an alternative mechanism may link the AKAP121 and DRP1 pathways in cardiac lipid overload.

Our data also reveals that substrate availability and mitochondrial dynamics plays an important role in the developmental maturation of mitochondria in the perinatal period. In fetal cardiomyocytes, energy substrate utilization mainly depends on lactate and glucose supplied from the maternal circulation. After birth, energy substrate utilization shifts rapidly from lactate oxidation and glycolysis to fatty acid oxidation in mitochondria, and cardiomyocytes preferentially utilize fatty acid as an energy source throughout their life.^{2, 34} In this process, mitochondria undergo profound remodeling in terms of shape and volume, which is accompanied by an increase in the activities of enzymes required for lipid oxidation, such as LCAD, MCAD, CPT1, and ACSL1.^{4, 35} The progressive post-natal increase in mitochondrial dimensions was absent in ACStg heart, which showed a multitude of apparently small

mitochondria occupying a larger fractional cell volume than WT. 3-D EM tomographic reconstructions revealed a narrow, elongated and tortuous morphology of mitochondria that is principally different from WT and which would be sectioned multiple times in a single plane. Our novel imaging methodology underscores the challenges in estimating mitochondrial size and number from 2-D images and adds new insight into the structural adaptations of mitochondria in the heart when signaling pathways that regulate mitochondrial dynamics are perturbed.

The substantial increase of fatty acid availability in the perinatal circulation activates PPAR α that drives fatty acid oxidation in mitochondria.^{36, 37} We show here that DRP1 phosphorylation is rapidly modulated during post-natal cardiac development. Furthermore, forced lipid uptake in the early post-natal period alters the developmental changes in DRP1 phosphorylation and prevented physiological and maturation-dependent mitochondrial fusion. An indispensable role of DRP1 in perinatal cardiac development has been recently reported.³⁸⁻⁴⁰ Taken together, post translational modifications of DRP1 after birth, plays an important role in normal perinatal mitochondrial maturation.

Along with the alteration of mitochondrial membrane dynamics, mitochondrial membrane lipid content was also affected in our cardiac lipid overload model. Although the detailed molecular mechanisms involved are incompletely understood, the lipid composition of cristae membrane, specifically cardiolipin and phospholipids, plays an important role in mitochondrial membrane fluidity, cristae structure and oxidative phosphorylation.⁴¹ Consistent with an elevation of cardiac ceramide and DAG levels (Fig. 1E, 1F), phospholipid composition and the side chain pattern of cardiolipin were significantly altered in ACStg mitochondrial membranes (Supplemental Fig. IX-A, IX-B). Interestingly, there was a significant reduction in tetralinoleic (18:2)⁴ cardiolipin (L4CL) (Supplemental Fig. IX-A). It is widely accepted that L4CL is the fully functional CL species and the reduction of L4CL has been associated with diabetes, heart failure, ischemia reperfusion injury, all of which are associated with impaired mitochondrial function.^{42, 43} These changes are due in part to an important role for cardiolipin in mitochondrial supercomplex formation and cytochrome oxidase activity.⁴⁴ Moreover, L4CL is thought to promote more efficient proton flow and as such the reduction observed in ACStg mice could account in part for the increased ROS generation.

We also addressed the contribution of increased ceramide content in altering mitochondrial morphology in our lipid overload model *in vivo* and *vitro*. Using myriocin, an inhibitor for serine-palmitoyl transferase, which catalyzes the first step of *de novo* ceramide synthesis, we

determined that the inhibition of *de novo* ceramide synthesis exacerbated ROS production in palmitate treated NRVCs (Supplemental Fig. X-A–E). Furthermore, *in vivo* inhibition of ceramide synthesis by heterozygous deletion of Des1, an enzyme that catalyzes *de novo* ceramide synthesis, failed to reverse the altered mitochondrial network (Supplemental Fig. X-F). These data indicate that increased ROS resulting from mitochondrial lipid oxidation likely represents a primary mechanism responsible for augmenting mitochondrial fission in lipid overload, and that ceramide accumulation does not contribute to this process.

In summary, we demonstrate here that increased myocardial lipid uptake impairs mitochondrial dynamics by increasing mitochondrial ROS generation, which modulates post-translational modification of OPA1 and DRP1 (Supplemental Fig. XI). We also provide evidence that mitochondrial dynamics is involved in perinatal mitochondrial maturation and forced lipid uptake interferes with that process. These findings add a new dimension to understanding the regulation of mitochondrial morphology and physiology in the heart and its dysregulation by lipid excess.

Author contributions — K.T., H.B., A.R.W., J.S., G.A.J., A.R.T., R.M., Y.Z., R.S., X.X.H., C.L.S., R.O.P., V.A.L., K.W.S., T.L.S., K.I.S G.C.S., P.K., E.R-Z and O.K performed experiments and analyzed the data; J.E.S. provided critical reagents and experimental guidance. K.T., H.B. and E.D.A. designed the study and prepared a draft of the manuscript. E.D.A. coordinated the project and the writing of the paper, to which all authors contributed.

Acknowledgments — We thank Dr. Elizabeth A. Amiot and Dr. Janet M. Shaw for providing critical reagents and experimental guidance in the L6 mitochondrial fusion assays; Heather Theobald for technical help, and Dr. Eric T. Weatherford and Mr. Paul Casella for the editing of the manuscript.

Sources of funding

Japan Heart Foundation/Bayer Yakuhin Research Grant Abroad (to K.T.)
American Heart Association Post-doctoral fellowship (12POST12030309) (to K.T.)
Deutsche Forschungsgemeinschaft (DFG) (to H.B.)
National Institute of Health (RO1 DK064989, P20 HL113444) (to J.E.S.)
National Institute of Health (UO1 HL087947, RO1HL108379) (to E.D.A.)
Juvenile Diabetes Research Foundation (to E.D.A.)
European Research Council Advanced Grant CardioNECT (20120314) (to P.K.).

Disclosures — The authors have declared no conflict of interest exists.

References

- Doenst T, Nguyen TD and Abel ED. Cardiac metabolism in heart failure: implications beyond ATP production. *Circ Res*. 2013;113:709-24.
- de Jong H, Neal AC, Coleman RA and Lewin TM. Ontogeny of mRNA expression and activity of long-chain acyl-CoA synthetase (ACSL) isoforms in *Mus musculus* heart. *Biochim Biophys Acta*. 2007;1771:75-82.
- Lopaschuk GD, Collins-Nakai RL and Itoi T. Developmental changes in energy substrate use by the heart. *Cardiovasc Res*. 1992;26:1172-80.
- Lopaschuk GD, Witters LA, Itoi T, Barr R and Barr A. Acetyl-CoA carboxylase involvement in the rapid maturation of fatty acid oxidation in the newborn rabbit heart. *J Biol Chem*. 1994;269:25871-8.
- Kolwicz SC, Jr., Purohit S and Tian R. Cardiac metabolism and its interactions with contraction, growth, and survival of cardiomyocytes. *Circ Res*. 2013;113:603-16.
- Duncan JG. Mitochondrial dysfunction in diabetic cardiomyopathy. *Biochim Biophys Acta*. 2011;1813:1351-9.
- Boudina S and Abel ED. Diabetic cardiomyopathy, causes and effects. *Rev Endocr Metab Disord*. 2010;11:31-9.
- Bugger H and Abel ED. Mitochondria in the diabetic heart. *Cardiovasc Res*. 2010;88:229-40.
- Zorzano A, Liesa M and Palacin M. Role of mitochondrial dynamics proteins in the pathophysiology of obesity and type 2 diabetes. *Int J Biochem Cell Biol*. 2009;41:1846-54.
- Boudina S, Sena S, Theobald H, Sheng X, Wright JJ, Hu XX, Aziz S, Johnson JJ, Bugger H, Zaha VG and Abel ED. Mitochondrial energetics in the heart in obesity-related diabetes: direct evidence for increased uncoupled respiration and activation of uncoupling proteins. *Diabetes*. 2007;56:2457-66.
- Boudina S, Bugger H, Sena S, O'Neill BT, Zaha VG, Ilkun O, Wright JJ, Mazumder PK, Palfreyman E, Tidwell TJ, Theobald H, Khalimonchuk O, Wayment B, Sheng X, Rodnick KJ, Centini R, Chen D, Litwin SE, Weimer BE and Abel ED. Contribution of impaired myocardial insulin signaling to mitochondrial dysfunction and oxidative stress in the heart. *Circulation*. 2009;119:1272-83.
- Belke DD, Betuing S, Tuttle MJ, Graveleau C, Young ME, Pham M, Zhang D, Cooksey RC, McClain DA, Litwin SE, Taegtmeyer H, Severson D, Kahn CR and Abel ED. Insulin signaling coordinately regulates cardiac size, metabolism, and contractile protein isoform expression. *J Clin Invest*. 2002;109:629-39.
- Chiu HC, Kovacs A, Ford DA, Hsu FF, Garcia R, Herrero P, Safitz JE and Schaffer JE. A novel mouse model of lipotoxic cardiomyopathy. *J Clin Invest*. 2001;107:813-22.
- Piquereau J, Novotova M, Fortin D, Garnier A, Ventura-Clapier R, Veksler V and Joubert F. Postnatal development of mouse heart: formation of energetic microdomains. *The Journal of physiology*. 2010;588:2443-54.
- Kanamaru Y, Sekine S, Ichijo H and Takeda K. The phosphorylation-dependent regulation of mitochondrial proteins in stress responses. *Journal of signal transduction*. 2012;2012:931215.
- Otera H, Ishihara N and Mihara K. New insights into the function and regulation of mitochondrial fission. *Biochim Biophys Acta*. 2013;1833:1256-68.
- Chang CR and Blackstone C. Cyclic AMP-dependent protein kinase phosphorylation of Drp1 regulates its GTPase activity and mitochondrial morphology. *J Biol Chem*. 2007;282:21583-7.
- Merrill RA and Strack S. Mitochondria: a kinase anchoring protein 1, a signaling platform for mitochondrial form and function. *Int J Biochem Cell Biol*. 2014;48:92-6.
- Carlucci A, Adornetto A, Scorziello A, Viggiano D, Foca M, Cuomo O, Annunziato L, Gottesman M and Feliciello A. Proteolysis of AKAP121 regulates mitochondrial activity during cellular hypoxia and brain ischaemia. *EMBO J*. 2008;27:1073-84.
- Kim H, Scimia MC, Wilkinson D, Trelles RD, Wood MR, Bowtell D, Dillin A, Mercola M and Ronai ZA. Fine-tuning of Drp1/Fis1 availability by AKAP121/Siah2 regulates mitochondrial adaptation to hypoxia. *Mol Cell*. 2011;44:532-44.
- Delettre C, Griffoin JM, Kaplan J, Dollfus H, Lorenz B, Faivre L, Lenaers G, Belenguer P and Hamel CP. Mutation spectrum and splicing variants in the OPA1 gene. *Hum Genet*. 2001;109:584-91.
- Ishihara N, Fujita Y, Oka T and Mihara K. Regulation of mitochondrial morphology through proteolytic cleavage of OPA1. *EMBO J*. 2006;25:2966-77.
- Wende AR and Abel ED. Lipotoxicity in the heart. *Biochim Biophys Acta*. 2010;1801:311-9.
- Russo SB, Baicu CF, Van Laer A, Geng T, Kasiganesan H, Zile MR and Cowart LA. Ceramide synthase 5 mediates lipid-induced autophagy and hypertrophy in cardiomyocytes. *J Clin Invest*. 2012;122:3919-30.
- Germain M, Mathai JP, McBride HM and Shore GC. Endoplasmic reticulum BIK initiates DRP1-regulated remodeling of mitochondrial cristae during apoptosis. *EMBO J*. 2005;24:1546-56.
- Murphy MP. How mitochondria produce reactive oxygen species. *Biochem J*. 2009;417:1-13.
- Mazumder PK, O'Neill BT, Roberts MW, Buchanan J, Yun UJ, Cooksey RC, Boudina S and Abel ED. Impaired cardiac efficiency and increased fatty acid oxidation in insulin-resistant ob/ob mouse hearts. *Diabetes*. 2004;53:2366-74.
- Bugger H, Boudina S, Hu XX, Tuinei J, Zaha VG, Theobald HA, Yun UJ, McQueen AP, Wayment B, Litwin SE and Abel ED. Type 1 diabetic akita mouse hearts are insulin sensitive but manifest structurally abnormal mitochondria that remain coupled despite increased uncoupling protein 3. *Diabetes*. 2008;57:2924-32.
- Montaigne D, Marechal X, Coisne A, Debry N, Modine T, Fayad G, Potelle C, El Arid JM, Mouton S, Sebt Y, Duez H, Preau S, Remy-Jouet I, Zerimech F, Koussa M, Richard V, Nevriere R, Edme JL, Lefebvre P and Staels B. Myocardial contractile dysfunction is associated with impaired mitochondrial function and dynamics in type 2 diabetic but not in obese patients. *Circulation*. 2014;130:554-64.
- Kashatus JA, Nascimento A, Myers LJ, Sher A, Byrne FL, Hoehn KL, Counter CM and Kashatus DF. Erk2 phosphorylation of

- Drp1 promotes mitochondrial fission and MAPK-driven tumor growth. *Mol Cell*. 2015;57:537-51.
31. Strack S, Wilson TJ and Cribbs JT. Cyclin-dependent kinases regulate splice-specific targeting of dynamin-related protein 1 to microtubules. *J Cell Biol*. 2013;201:1037-51.
 32. Taguchi N, Ishihara N, Jofuku A, Oka T and Mihara K. Mitotic phosphorylation of dynamin-related GTPase Drp1 participates in mitochondrial fission. *J Biol Chem*. 2007;282:11521-9.
 33. Norton M, Ng AC, Baird S, Dumoulin A, Shutt T, Mah N, Andrade-Navarro MA, McBride HM and Screatton RA. ROMO1 is an essential redox-dependent regulator of mitochondrial dynamics. *Science signaling*. 2014;7:ra10.
 34. Makinde AO, Kantor PF and Lopaschuk GD. Maturation of fatty acid and carbohydrate metabolism in the newborn heart. *Mol Cell Biochem*. 1998;188:49-56.
 35. Nagao M, Parimoo B and Tanaka K. Developmental, nutritional, and hormonal regulation of tissuespecific expression of the genes encoding various acyl-CoA dehydrogenases and alpha-subunit of electron transfer flavoprotein in rat. *J Biol Chem*. 1993;268:24114-24.
 36. Barger PM and Kelly DP. PPAR signaling in the control of cardiac energy metabolism. *Trends Cardiovasc Med*. 2000;10:238-45.
 37. Lehman JJ, Barger PM, Kovacs A, Saffitz JE, Medeiros DM and Kelly DP. Peroxisome proliferator-activated receptor gamma coactivator-1 promotes cardiac mitochondrial biogenesis. *J Clin Invest*. 2000;106:847-56.
 38. Ishihara T, Ban-Ishihara R, Maeda M, Matsunaga Y, Ichimura A, Kyogoku S, Aoki H, Katada S, Nakada K, Nomura M, Mizushima N, Mihara K and Ishihara N. Dynamics of mitochondrial DNA nucleoids regulated by mitochondrial fission is essential for maintenance of homogeneously active mitochondria during neonatal heart development. *Molecular and cellular biology*. 2015;35:211-23.
 39. Ikeda Y, Shirakabe A, Maejima Y, Zhai P, Sciarretta S, Toli J, Nomura M, Mihara K, Egashira K, Ohishi M, Abdellatif M and Sadoshima J. Endogenous Drp1 mediates mitochondrial autophagy and protects the heart against energy stress. *Circ Res*. 2015;116:264-78.
 40. Kageyama Y, Hoshijima M, Seo K, Bedja D, Sysa-Shah P, Andrabi SA, Chen W, Hoke A, Dawson VL, Dawson TM, Gabrielson K, Kass DA, Iijima M and Sesaki H. Parkin-independent mitophagy requires Drp1 and maintains the integrity of mammalian heart and brain. *The EMBO journal*. 2014;33:2798-813.
 41. Shen Z, Ye C, McCain K and Greenberg ML. The Role of Cardiolipin in Cardiovascular Health. *Biomed Res Int*. 2015;2015:891707.
 42. Sparagna GC, Chicco AJ, Murphy RC, Bristow MR, Johnson CA, Rees ML, Maxey ML, McCune SA and Moore RL. Loss of cardiac tetralinoleoyl cardiolipin in human and experimental heart failure. *J Lipid Res*. 2007;48:1559-70.
 43. Sparagna GC, Johnson CA, McCune SA, Moore RL and Murphy RC. Quantitation of cardiolipin molecular species in spontaneously hypertensive heart failure rats using electrospray ionization mass spectrometry. *J Lipid Res*. 2005;46:1196-204.
 44. Shinzawa-Itoh K, Aoyama H, Muramoto K, Terada H, Kurauchi T, Tadehara Y, Yamasaki A, Sugimura T, Kurono S, Tsujimoto K, Mizushima T, Yamashita E, Tsukihara T and Yoshikawa S. Structures and physiological roles of 13 integral lipids of bovine heart cytochrome c oxidase. *EMBO J*. 2007;26:1713- 25.

Novelty and Significance

What Is Known?

- Obesity and diabetes induce myocardial lipotoxicity that may reduce cardiac function.
- Cardiac lipotoxicity is associated with mitochondrial dysfunction including decreased oxidative phosphorylation via incompletely understood mechanisms.

What New Information Does This Article Contribute?

- Myocardial lipid overload by saturated fatty acids (FA) transiently increases mitochondrial respiration, membrane potential and ROS production.
- FA-induced mitochondrial ROS overproduction induces post-translational modifications of mitochondrial fusion/fission regulatory proteins that precipitate increased mitochondrial fission.
- 3D-electron tomography revealed that lipid overload in post-natal hearts induces ROS-mediated fragmentation of the mitochondrial network, characterized by narrow tortuous and tubular morphology.

Obesity, insulin resistance and diabetes are associated with increased fatty acids (FAs) utilization and reduced glucose utilization. One proposed mechanism for cardiac dysfunction called "lipotoxicity" is excess intracellular lipid accumulation secondary to a mismatch between lipid supply and utilization. In this study, using a mouse model with increased myocardial lipid uptake, we demonstrate that myocardial lipid overload induces mitochondrial ROS production, which alters the activity of DRP1 and OPA1, leading to fragmentation of the mitochondrial network characterized by a narrow tubular morphology. Thus, dysregulation of mitochondrial dynamics following lipid overload may represent an important mechanism contributing to mitochondrial and contractile dysfunction in lipotoxic cardiomyopathies.

Supplemental Materials

Methods

Animal model

Mice with cardiomyocyte-restricted low-level overexpression of long-chain acyl-CoA synthetase 1 (ACStg) and control littermates (WT) were originally on the FVB background¹. We prepared a transgenic line on the C57BL6j background by backcrossing more than 8 generations. DRP1 floxed mice (Kind gift of Hiromi Sesaki, Johns Hopkins University, Baltimore MD) were used to generate cardiomyocyte-restricted heterozygous deletions of DRP1 (Mixed Background). Sod2 transgenic mice (FVB background) were a kind gift from Paul Epstein (University of Louisville, Louisville, KY) and Des1 +/- mice (C57BL6 background) were a kind gift of Scott Summers (University of Utah, Salt Lake City, UT). Animals were studied in accordance with protocols approved by the Institutional Animal Care and Use Committees of the University of Utah and the Carver College of Medicine of the University of Iowa. All mice were housed at 22°C with free access to water and food (standard chow diet) with a light cycle of 12h light and 12h dark.

In vivo cardiac function

Echocardiography or left-ventricular (LV) catheterization was performed in a subset of the mice before respiration studies as described previously.² Mice were lightly anesthetized with isoflurane and imaged in the left lateral decubitus position with a linear 13-MHz probe (Vivid V echocardiograph; GE Healthcare, Tampa, FL). Cardiac dimensions and function were calculated from these digital images. Invasive LV hemodynamic measurements were performed with a temperature-calibrated 1.4-Fr micromanometer-tipped catheter (Millar Instruments, Houston, TX) inserted through the right carotid artery in mice anesthetized with chloral hydrate (400 mg/kg) and analyzed as described by us previously.

In vivo palmitate uptake

In vivo palmitate uptake was measured by quantifying cardiac palmitate biodistribution of 1-¹¹C-palmitate using

small-animal positron emission tomography (PET) as described before.³

***In vivo* MG132 administration** 10mg of MG132 (EMD Millipore, Billerica, MA) was dissolved in Corn Oil (Sigma-Aldrich, St. Louis, MO) by rotating 24hrs in room temperature. MG132 (10mg/kg body weight) was administered intraperitoneally twice, prior to euthanasia (- 18h and - 6h).

Cardiomyocyte isolation

Primary cultures of neonatal rat ventricular cardiomyocytes (NRVCs) were prepared from the ventricles of 3-5-day-old Wistar rats as described previously.⁴ NRVCs were plated on type I collagen coated cover glass or culture plates and incubated with DMEM supplemented with BSA or palmitate-BSA. NRVCs were also infected with adenovirus expressing either Ad-GFP or Ad-DRP1K38E at 10 MOI. The CRP-DRP1-K38E adenovirus was a gift from Dr. Ruth Slack's laboratory, Ottawa, Canada.⁵ After 12hr. of infection, NRVCs were incubated in DMEM or palmitate as described above.

Mitochondrial fusion assay

Mitochondrial fusion was investigated using the PEG fusion assay, as described before with minor modifications⁶. In brief, L6 myoblasts were infected with mitoGFP or mitoRFP (kind gifts from Dr. D. Chan) using retrovirus infection, and 25,000 cells expressing mitoGFP or mitoRFP were co-plated on 18mm coverslips in 6-well plates. Fusion was initiated by adding 300 µl of 50% PEG 1500 (Roche, Indianapolis, IN) for 60s, followed by addition of 2ml DMEM and two more washing steps with DMEM. Cells were incubated with 1ml cycloheximide (30 µg/ml) for 8 h, washed with 1X PBS, and fixed with 3.7% formaldehyde. Cells were viewed on a FluoView FV1000 confocal microscope (Olympus, Tokyo, Japan) at a magnification of 630x.

Immunofluorescence

Adult cardiomyocytes and neonatal rat ventricular cardiomyocytes were isolated as described before.⁷ For mitochondrial staining of adult cardiomyocytes, cells were incubated in HEPES buffer (126mM NaCl, 4.4mM KCl, 1.0mM, MgCl₂, 1.08mM CaCl₂, 11mM dextrose, 0.5mM

probenecid, 24mM HEPES, pH 7.4) containing 100nM of the fluorescent potential-dependent indicator, tetramethylrhodamine ethyl ester (TMRE; Molecular Probes, Eugene, OR), for 30min at 37°C. Cells were then placed into a glass-bottom perfusion chamber mounted on a Zeiss LSM 510 confocal microscope (Zeiss, Oberkochen, Germany), perfused with HEPES-buffer at 37°C, and viewed. For neonatal rat ventricular cardiomyocytes grown on coverslips, cells were washed in warm PBS, fixed in 4% paraformaldehyde in PBS (15 min in room temperature), then washed in PBS, permeabilized with 0.2% TritonX in PBS (10 min in room temperature) and blocked in blocking solution (5% BSA in PBS with 0.05% Tween20, 30 min in room temperature). Antibody labeling was performed by addition of 200 µl blocking solution with primary or secondary antibodies (1–5 µg/ml) and washing with PBS containing 0.05% Tween20. Samples were mounted in 40% glycerol/PBS on glass slides and sealed with clear nail polish. Images were acquired in an Olympus FV-1000 confocal microscope or a Zeiss LSM 710 confocal microscope. The following antibodies were used for immunohistochemistry: Tom20 (Santa Cruz Biotechnology, Dallas, TX, sc-11415), α -actinin (Sigma-Aldrich, A7811) and DRP1 (Novus Biologicals, Littleton, CO, h00010059-m01).

Mitochondrial function

Mitochondrial oxygen consumption and ATP synthesis rates were measured in saponin permeabilized fibers using palmitoyl-carnitine/malate, pyruvate/malate, or glutamate/malate as substrate combinations, as described before.⁸ Mitochondria were isolated by differential centrifugation, and oxygen consumption and ATP synthesis were measured using palmitoyl-carnitine/malate, pyruvate/malate, or glutamate/malate as substrate combinations, as described before.⁹ OXPHOS complexes of isolated mitochondrial membranes were separated by blue-native gel electrophoresis, and complex activities were determined by in-gel staining assays, as described before.⁹ Mitochondrial respiration rate in NRVCs were assessed using a Seahorse XFp Extracellular Flux Analyzer with the XFp Cell Mito Stress Test Kit (Agilent, Santa Clara, CA). In brief, NRVCs were plated at 75,000 cells/well in a 24-well Seahorse assay plate and maintained for 48hrs with DMEM (5.5mM glucose, 10 µM AraC, 5% FBS and 10% horse serum). 24hr before the assay, media was changed to DMEM (5.5mM glucose without AraC and serum) and subjected to Seahorse analysis with DMEM (5.5mM glucose) supplemented with BSA or fatty acid-conjugated BSA.

Mitochondrial membrane potential assay

Mitochondrial membrane potential in NRVCs was measured by TMRM fluorescence intensity. In brief, NRVCs were plated at 50,000 cells/well in a 96-well black bottom dish. After palmitate stimulation, NRVCs were incubated with 10 µM TMRM and 100µg/ml Hoechst for 30min at 37°C. TMRM (540/580) and Hoechst (360/450) fluorescence intensity was measured by a SpectraMax3 plate reader (Molecular devices, Sunnyvale, California). The TMRM/Hoechst fluorescence ratio is used to determine the mitochondrial membrane potential.

ATP extraction and quantification

ATP content in NRVCs was measured by an ENLITEN ATP Assay System Bioluminescence Detection Kit for ATP Measurement (Promega, Madison, WI). In brief, NRVCs were plated in a 96-well plate at a density of 50,000 cells/well. ATP was extracted with 50 µl of TCA (1%)/EDTA(4mM) buffer.

Oxidative stress and superoxide production

Mitochondrial H₂O₂ production was measured with a fluorometric assay as described before.⁸ Activity of aconitase was measured in isolated mitochondria using a spectrophotometric assay, and tissue ROS levels were measured by the conversion of nonfluorescent 2',7'-dichlorofluorescein-diacetate (DCFDA) to the highly fluorescent 2',7'-dichlorofluorescein (DCF), as described before.⁸ In NRVCs, ROS levels were measured by CellRox Green reagent in accordance with the manufacturer's instructions (Thermo Fisher Scientific, Waltham, MA).

Quantification of mitochondrial dimension and volume density in 2D electron microscopy

Samples for transmission electron microscopy were collected from left ventricular myocardium and fixed in 2.5% glutaraldehyde/1% paraformaldehyde, post-fixed in 2% osmium tetroxide, embedded in resin, and sectioned (80–100 nm thick), as described before.⁸ Mitochondrial volume density and dimensions of their two-dimensional (2D) cross-section were analyzed by 2D-stereology in a blinded fashion using the point counting method.⁸ Briefly, the image obtained at 3,000x magnification was overlaid

with square grids. Mitochondrial volume density was calculated by a number of grids superimposed over mitochondria. Apparent mitochondria size was calculated as volume density / mitochondrial number.

Electron microscopy and tomography

Hearts were Langendorff-perfused with Tyrode's solution containing 139mM NaCl, 3mM KCl, 17mM NaHCO₃, 12mM D-(+)-glucose, 3mM CaCl₂ and 1mM MgCl₂ and cardioplegically arrested using a high-K⁺ (25 mM) no-Ca²⁺ modified Tyrode's solution. Cardioplegically arrested hearts were perfusion-fixed with iso-osmotic Karnovsky's fixative (2.4% sodium cacodylate, 0.75% paraformaldehyde, 0.75% glutaraldehyde; 300 mOsm). Tissue fragments were excised from the left ventricle and washed with 0.1 M sodium cacodylate, post-fixed in 1% OsO₄ for 1 h, dehydrated in graded acetone, and embedded in Epon-Araldite resin. Thin (80 nm) and semi-thick (280 nm) sections were placed on formvar-coated slot-grids, post stained with 2% aqueous uranyl acetate and Reynold's lead citrate. Colloidal gold particles (15 nm) were added to both surfaces of the semi-thick sections to serve as fiducial markers for tilt-series alignment. Preparations were imaged at the EMBL Heidelberg Electron Microscopy Core Facility using a Tecnai F30 electron microscope operating at 300 kV and Philips CM120 BioTwin electron microscope operating at 120 kV. Images were captured on a 4K Eagle camera and SIS 1K KeenView, respectively.

For tomography, the SerialEM software package was used. The specimen holder was tilted from +60° to -60° at 1° intervals, followed by 90° rotation in the X-Y plane and a second round of acquisition (dual axis tilt). The images from each tilt-series were aligned by fiducial marker tracking and back-projected to generate two single full-thickness reconstructed volumes (tomograms), which were then combined to generate a single high-resolution 3D reconstruction of the original partial cell volume. Isotropic voxel size was 1.25 nm. All tomograms were processed and analysed using IMOD software, which was also used to generate 3D models of relevant structures of interest.¹⁰

Immunoblot analysis

Mitochondrial and cytosolic fractions were generated by homogenizing freshly excised hearts in homogenization buffer (20mM HEPES, 140mM KCl, 10mM EDTA, 5mM

MgCl₂, pH 7.4) with a Dounce tissue homogenizer, centrifuging the homogenate at 800x g for 10min, and centrifuging the resulting supernatant at 8,000 x g for 10min. The supernatant is the cytosolic fraction. The pellet was washed by centrifugation at 10,000 x g and represents the mitochondrial fraction. Whole-cell extracts and mitochondrial membranes were prepared as described before.¹¹ Samples were loaded on SDS-PAGE, transferred to nitrocellulose or PVDF membranes, and incubated with specific antibodies. Bands were visualized using horseradish peroxidase-conjugated secondary antibodies and the ECL detection system (GE Healthcare, Piscataway, NJ), or fluorophore-conjugated secondary antibodies and the Odyssey fluorescence detection system (Li-Cor Biosciences, Alpharetta, GA). The following antibodies were used for immunoblotting: ACSL1 (Cell Signaling Technology, Boston, MA, #4047), phospho- ERK1/2 (Cell Signaling Technology, #9101), phospho-SAPK/JNK (Cell Signaling Technology, #9251), DRP1 pS616 (Cell Signaling Technology, #3455), DRP1 pS637 (Cell Signaling Technology, #6319), DRP1 (Novus Biologicals, h00010059- m01), 4-Hydroxynoneal (4HNE) (Abcam, Cambridge, MA, ab46545), Mitofusin 1 (Abcam, ab57602), OPA1 (BD Biosciences, San Jose, CA, #612606), Mitofusin 2 (Sigma-Aldrich, M6319), Fis1 (Enzo Life Sciences, Farmingdale, NY, ALX-210- 1037-0100), MnSOD (Enzo Life Sciences, ADI-SOD-110-D).

Cardiac mitochondrial lipid analysis

For mass spectrometry sample preparation, tissue pieces were homogenized with a glass on glass homogenizer in PBS and lipids extracted according to a modified Bligh and Dyer method^{12, 13} using 1,000 nmol tetramyristal cardiolipin as an internal standard (Avanti Polar Lipids). Cardiolipin was quantified using our previously published methods¹² using liquid chromatography coupled to electrospray ionization mass spectrometry in an API 4000 mass spectrometer.

Statistical analysis

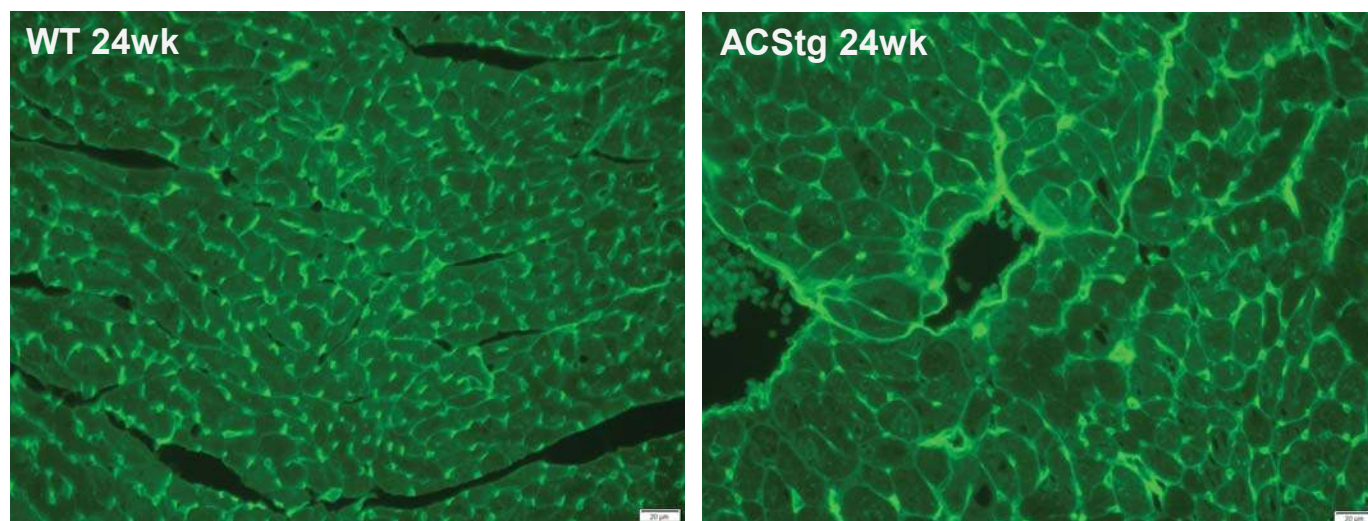
Results are presented as means ± SEM. Data were analyzed using unpaired student T-tests. If more than two groups were compared, 1-way ANOVA was performed, and significance was assessed using Fisher's protected least significance difference test. For T-tests and ANOVA, the Graphpad and Statplus software package was used (SAS Institute, Cary, NC). For all statistical analyses, significant difference was accepted when $P < 0.05$.

Supplemental References

1. Chiu HC, Kovacs A, Ford DA, Hsu FF, Garcia R, Herrero P, Safitz JE and Schaffer JE. A novel mouse model of lipotoxic cardiomyopathy. *J Clin Invest.* 2001 ; 107 :813-22.
2. Hu P, Zhang D, Swenson L, Chakrabarti G, Abel ED and Litwin SE. Minimally invasive aortic banding in mice: effects of altered cardiomyocyte insulin signaling during pressure overload. *Am J Physiol Heart Circ Physiol.* 2003;285:H1261-9.
3. Chiu HC, Kovacs A, Blanton RM, Han X, Courtois M, Weinheimer CJ, Yamada KA, Brunet S, Xu H, Nerbonne JM, Welch MJ, Fettig NM, Sharp TL, Sambandam N, Olson KM, Ory DS and Schaffer JE. Transgenic expression of fatty acid transport protein 1 in the heart causes lipotoxic cardiomyopathy. *Circ Res.* 2005;96:225-33.
4. Chien KR, Sen A, Reynolds R, Chang A, Kim Y, Gunn MD, Buja LM and Willerson JT. Release of arachidonate from membrane phospholipids in cultured neonatal rat myocardial cells during adenosine triphosphate depletion. Correlation with the progression of cell injury. *J Clin Invest.* 1985;75: 1770-80.
5. Germain M, Mathai JP, McBride HM and Shore Gc. Endoplasmic reticulum ERK initiates DRPI-regulated remodelling of mitochondrial cristae during apoptosis. *EMBO J* 2005;24:1546-56.
6. Chen H, Detmer SA, Ewald AJ, Griffin EE, Fraser SE and Chan DC. Mitofusins Mfn 1 and Mfn2 coordinately regulate mitochondrial fusion and are essential for embryonic development. *J Cell Biol.* 2003; 160: 189-200.
7. Mazumder PK, O'Neill BT, Roberts MW, Buchanan J, Yun VJ, Cooksey RC, Boudina S and Abel ED. Impaired cardiac efficiency and increased fatty acid oxidation in insulin-resistant ob/ob mouse hearts. *Diabetes* 2004;53:2366-74.
8. Bugger H, Boudina S, Hu XX, Tuinei J, Zaha VG, Theobald HA, Yun VJ, McQueen AP, Wayment B, Litwin SE and Abel ED. Type 1 diabetic akita mouse hearts are insulin sensitive but manifest structurally abnormal mitochondria that remain coupled despite increased uncoupling protein 3. *Diabetes* 2008;57:2924-32.
9. Boudina S, Bugger H, Sena S, O'Neill BT, Zaha VG, Ilkun O, Wright JJ, Mazumder PK, Palfreyman E, Tidwell TJ, Theobald H, Khalimonchuk O, Wayment B, Sheng X, Rodnick KJ, Centini R, Chen D, Litwin SE, Weimer BE and Abel ED. Contribution of impaired myocardial insulin signaling to mitochondrial dysfunction and oxidative stress in the heart. *Circulation.* 2009;119:1272-83.
10. Rog-Zielinska EA, Johnston CM, O'Toole ET, Morphew M, Hoeniger A. and Kohl P. Electron tomography of rabbit cardiomyocyte three-dimensional ultrastructure. *Prog Biophys Mol Biol* 2016;121:77-84.
11. Boudina S, Sen a S, O'Neill BT, Tathireddy P, Young ME and Abel ED. Reduced mitochondrial oxidative capacity and increased mitochondrial uncoupling impair myocardial energetics in obesity. *Circulation.* 2005;112:2686-95.
12. Sparagna GC, Johnson CA, McCune SA, Moore RL and Murphy RC. Quantitation of cardiolipin molecular species in spontaneously hypertensive heart failure rats using electrospray ionization mass spectrometry. *J Lipid Res.* 2005;46: 1196-204.
13. Bligh EG and Dyer WJ. A rapid method of total lipid extraction and purification. *Can J Biochem Physiol* 1959;37 :911-7.

Supplemental figures follow ...

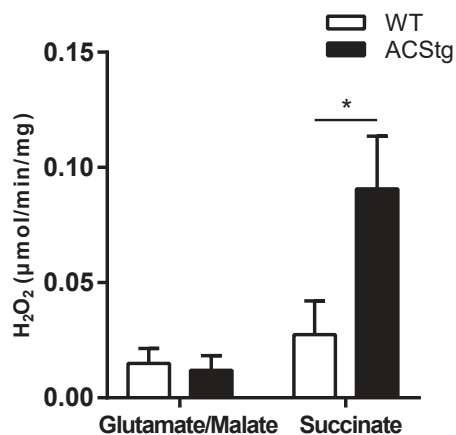
Supplemental Figure I



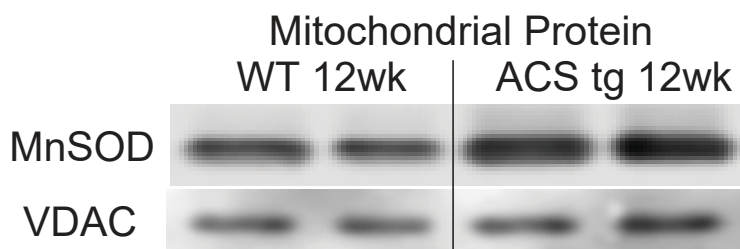
Representative images of wheat germ agglutinin staining of transverse heart sections obtained from 24-week-old ACStg mice and age-matched controls. Myocyte cross-sectional area were calculated from these images and presented in Figure 1H. Scale bars indicate 20 μ m.

Supplemental Figure II

(A)



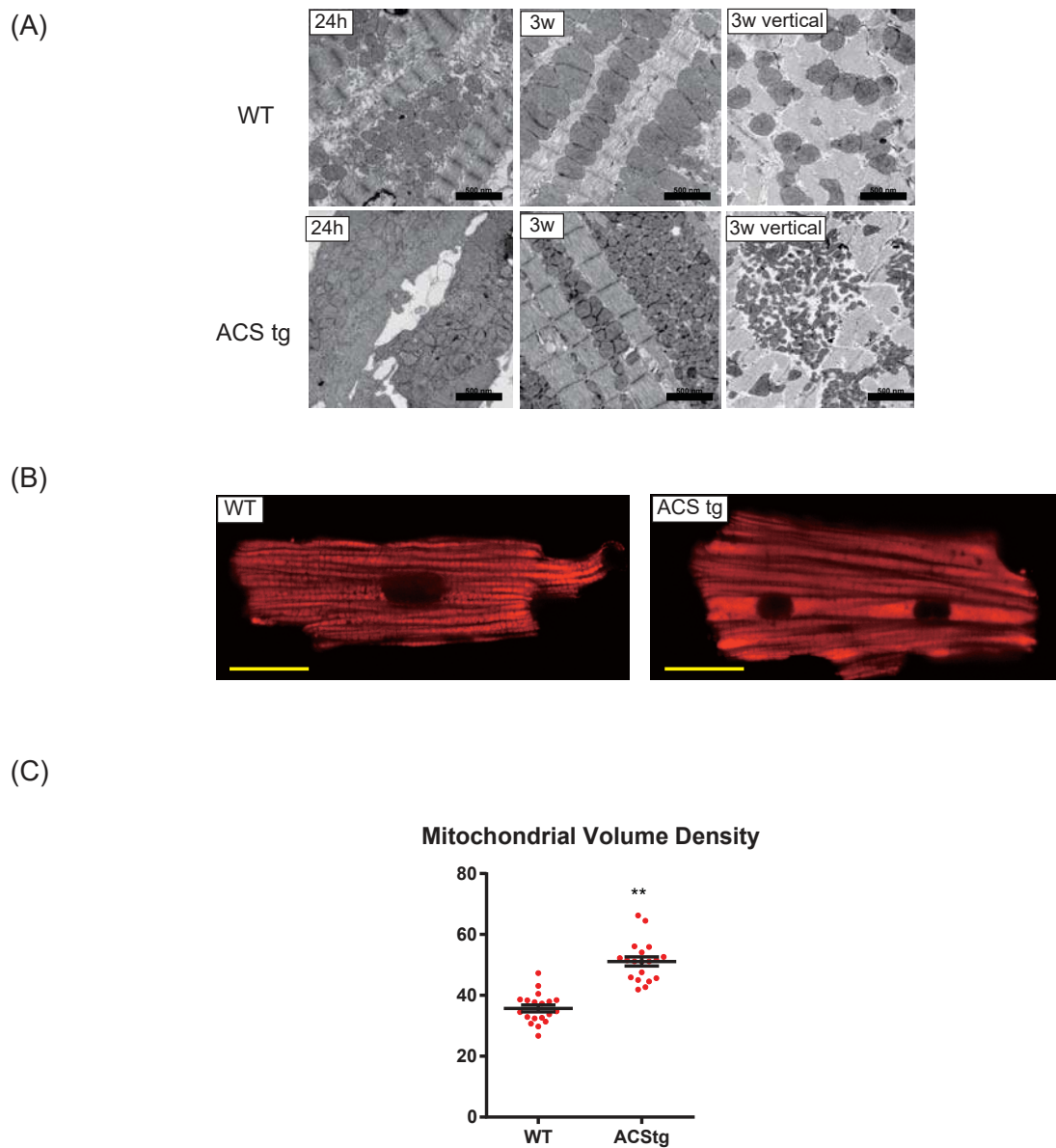
(B)



(A) H_2O_2 production with glutamate or succinate as a substrate in mitochondria isolated from 12-week-old WT and ACStg hearts. $n=3$, *; $P<0.05$.vs.WT

(B) Western blot of mitochondrial protein isolated from WT and ACStg hearts. Mitochondrial content of superoxide dismutase (SOD2 or MnSOD) and VDAC protein in 12-week-old WT and ACStg mice.

Supplemental Figure III



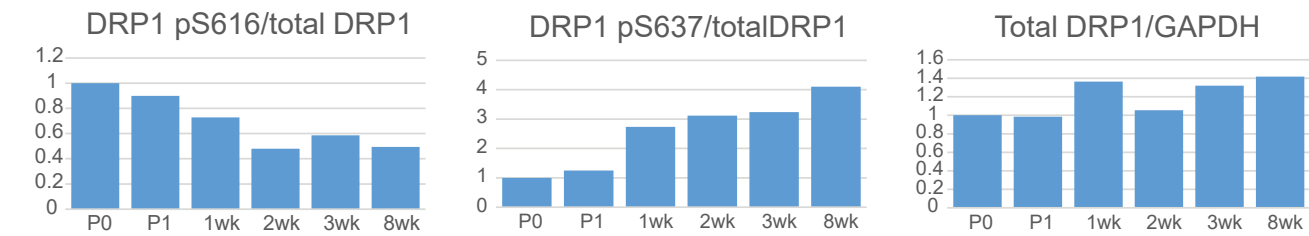
(A) Representative electron micrographs of longitudinal (24 hours, 3 weeks) or transverse (vertical) sections of WT and ACS tg hearts. Scale bars indicate 500nm.

(B) Representative confocal images of cardiomyocytes isolated from 12-week-old WT and ACS tg hearts, loaded with TMRE for 30 min. Scale bars indicate 20µm.

(C) Mitochondrial volume density was measured in 19 electron tomograms from 3 hearts per genotype; ** $P < 0.01$.

Supplemental Figure IV

(A)



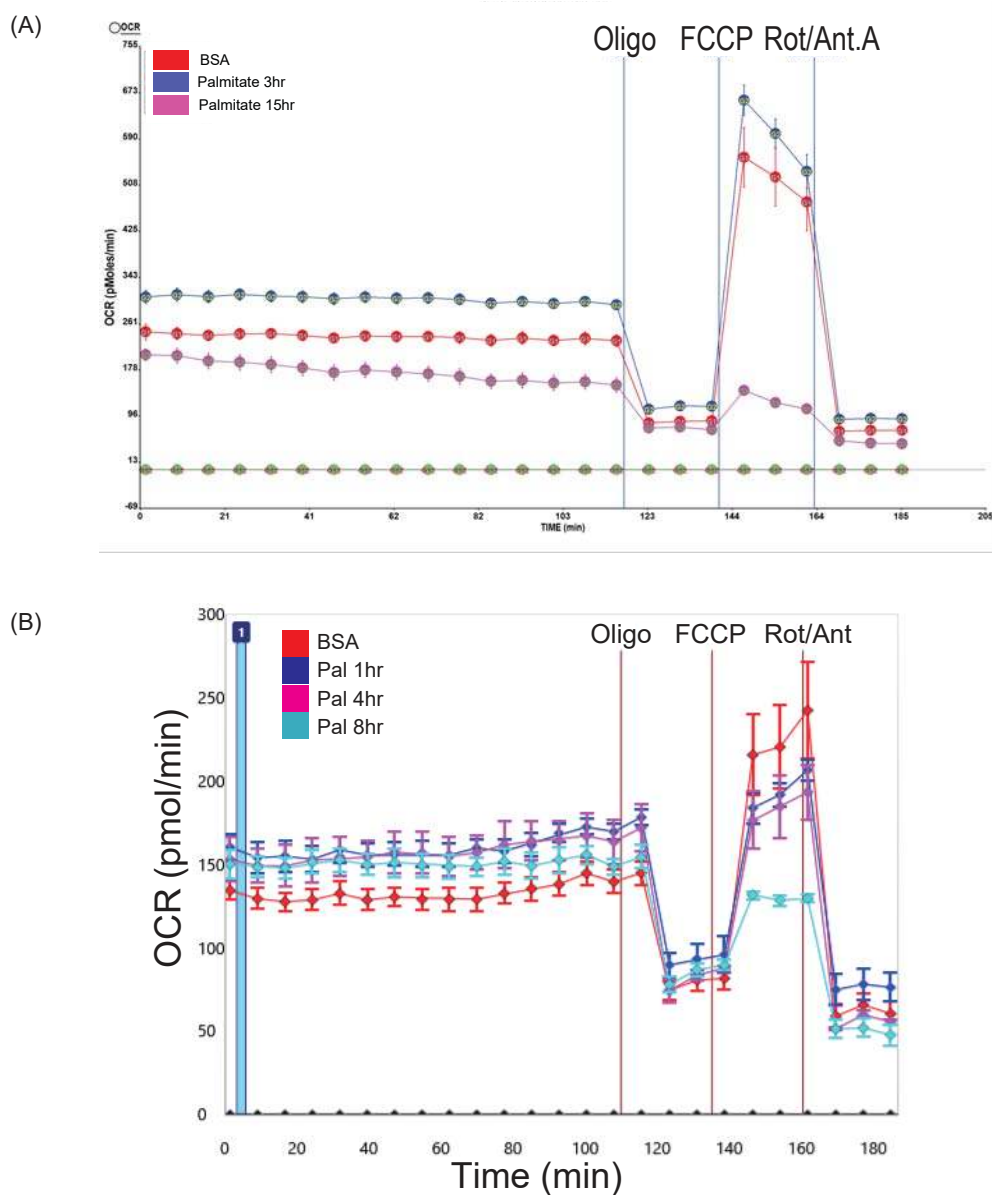
(B)



(A) Quantification of western blot presented in Figure 3G. Postnatal change of DRP1 phosphorylation in Wild-type whole heart homogenates.

(B) Quantification of western blot presented in Figure 3H. Postnatal change of DRP1 phosphorylation was compared between Wild-type and ACS transgenic mouse hearts.

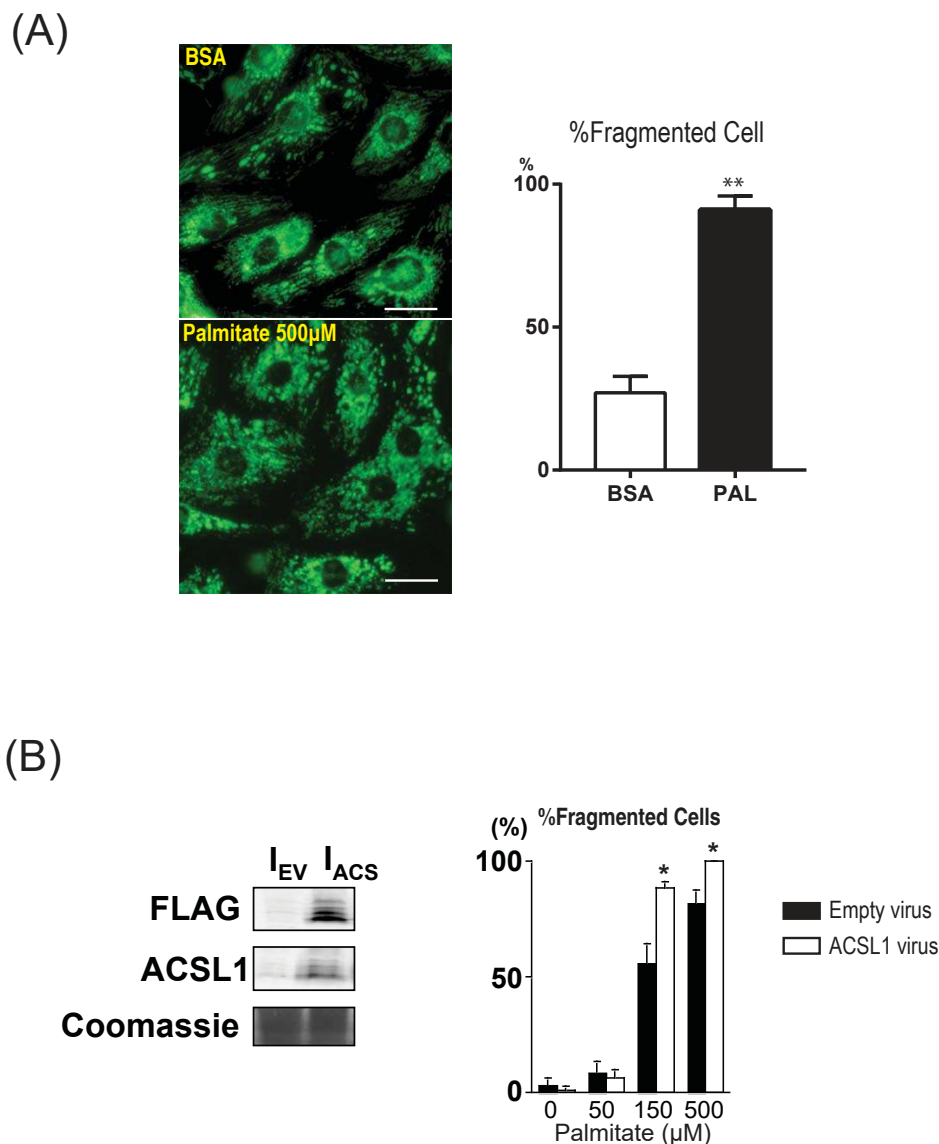
Supplemental Figure V



(A) NRVCs were pretreated with BSA or palmitate (500 μ M) for 3h or 15h as indicated and oxygen consumption rate (OCR) was measured with the XF24 Extracellular Flux Analyzer (Seahorse Bioscience). Oligomycin (4 μ M), FCCP (1 μ M) + Antimycin A (1 μ M) were sequentially added (indicated by lines). Short term palmitate treatment (3h) increased basal and maximum OCR. However, long term palmitate treatment (15h) decreased basal and maximum OCR.

(B) NRVCs were pre-treated with BSA or palmitate (500 μ M) for 1h, 4h or 8h as indicated and OCR was measured with the XF24 Extracellular Flux Analyzer. Basal OCR was increased by palmitate treatment. Reduced maximum OCR was observed after 8h of palmitate treatment.

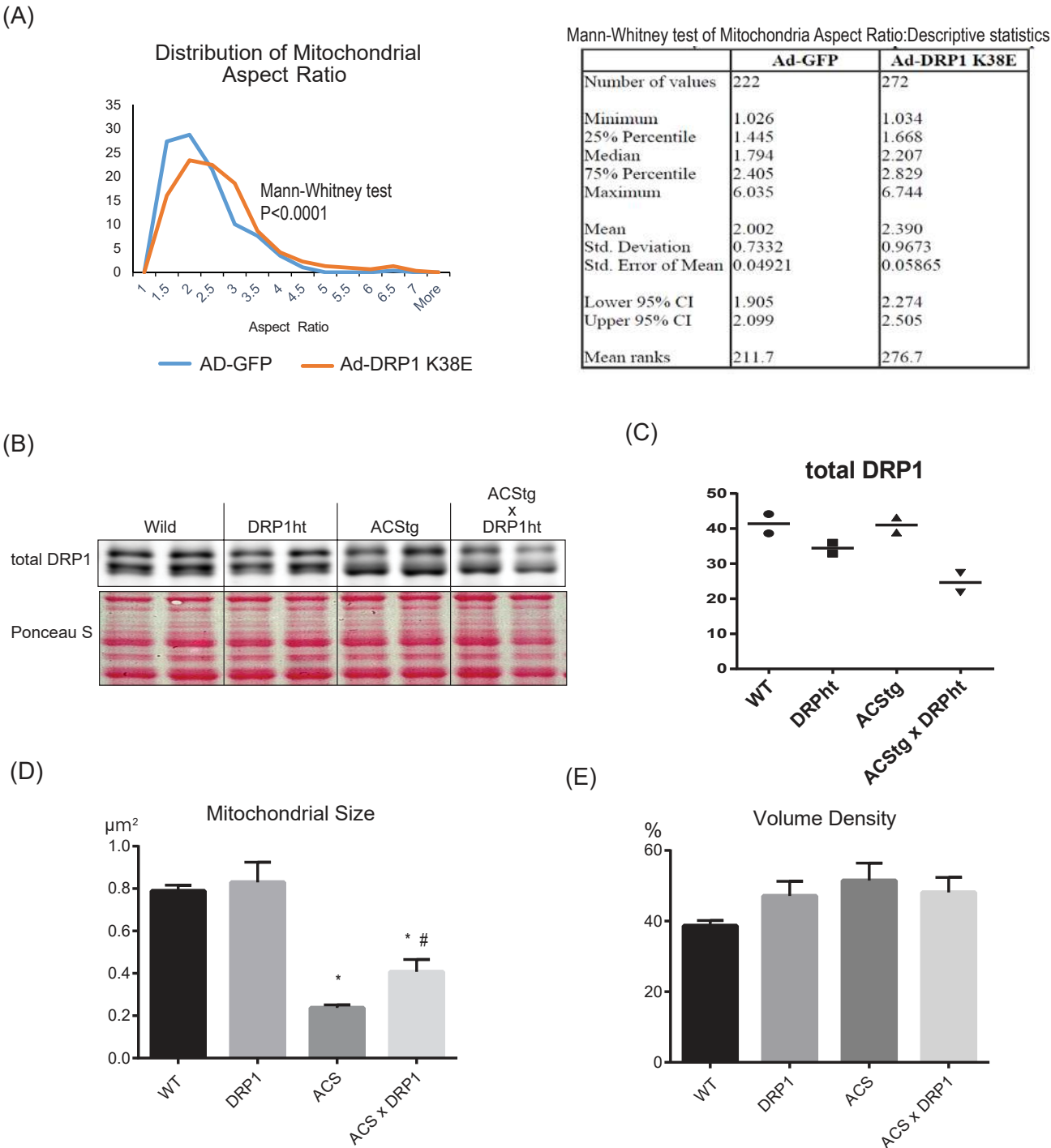
Supplemental Figure VI



(A) Rat neonatal cardiomyocytes were incubated with culture medium supplemented with BSA or BSA conjugated palmitate (500μM) for 12-hours. Mitochondria were stained with Mitotracker green according to the manufacturer's protocol. **; $P < 0.01$ vs. WT, Scale bars indicate 20μm.

(B) A representative Western blot for FLAG and ACSL1. I_{EV} - lysate of L6 cells transfected with empty virus; I_{ACS} - lysate of L6 cells transfected with ACSL1 virus. Cells infected with empty virus or ACSL1 virus were incubated in high-glucose DMEM + 10% FBS + 1% penicillin/streptomycin in the absence or presence of 500μM palmitate for 5 hours. Cells were evaluated to contain a tubular or fragmented mitochondrial network, and cells with fragmented mitochondria were expressed as percentage of all viewed cells $n=4$, * $p<0.05$ vs. Empty virus.

Supplemental Figure VII



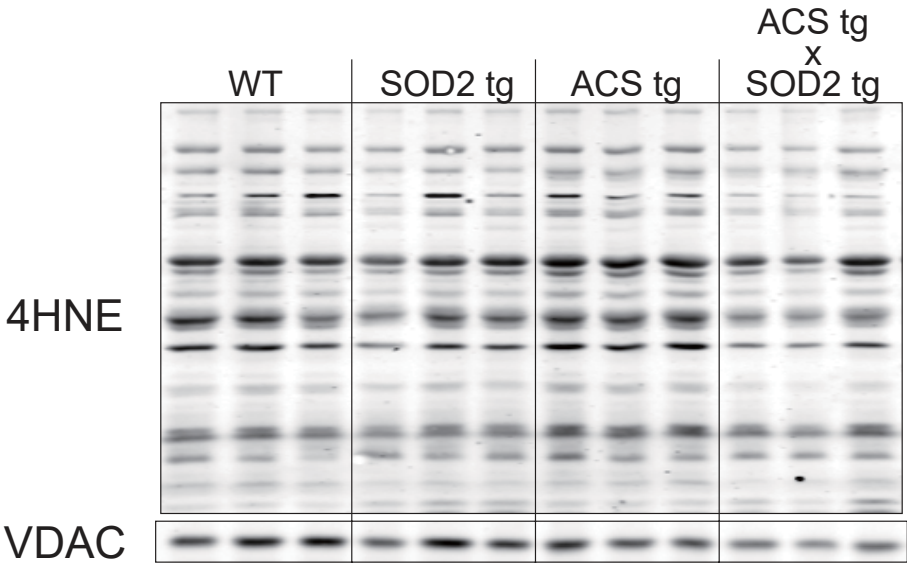
(A) Quantification of confocal images shown in Figure 6E. Mitochondrial aspect ratio was quantified by ImageJ as shown previously (Koopman et al., 2008).

(B-C) Western blot images of DRP1 protein content in whole heart lysates of Wild-type (WT), DRP1^{+/-} (DRP1ht), ACStg and compound mutant mice (B) and densitometric quantification of the immunoblot (C).

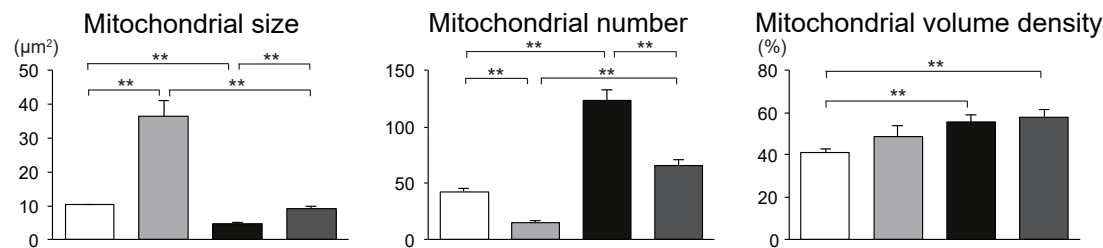
(D-E) Stereologic quantification of mitochondria size (D) and volume density (E) in WT, DRP1ht, ACStg and ACStg x

Supplemental Figure VIII

(A)



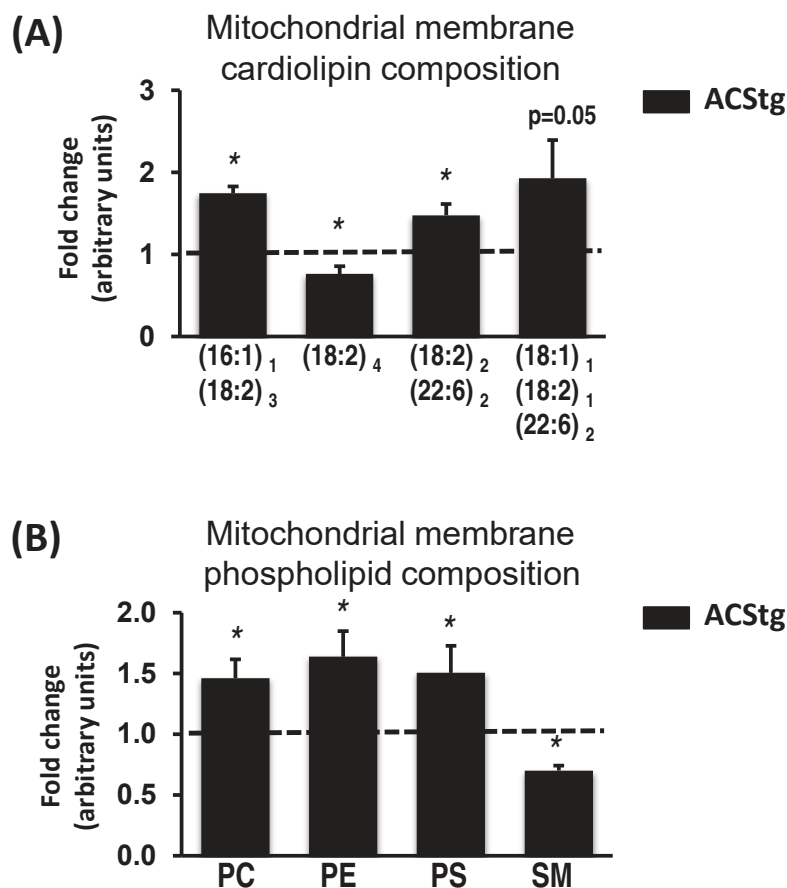
(B)



(A) Mitochondrial fractions were prepared from 12-week-old WT, SOD2tg, ACStg and SOD2 x ACS double transgenic hearts and subjected to western blot for 4HNE

(B) Quantification of mitochondrial size obtained by blind counting of 2 equivalent sections from each of three separate hearts in each group depicted in Figure 6F ** P <0.01.

Supplemental Figure IX

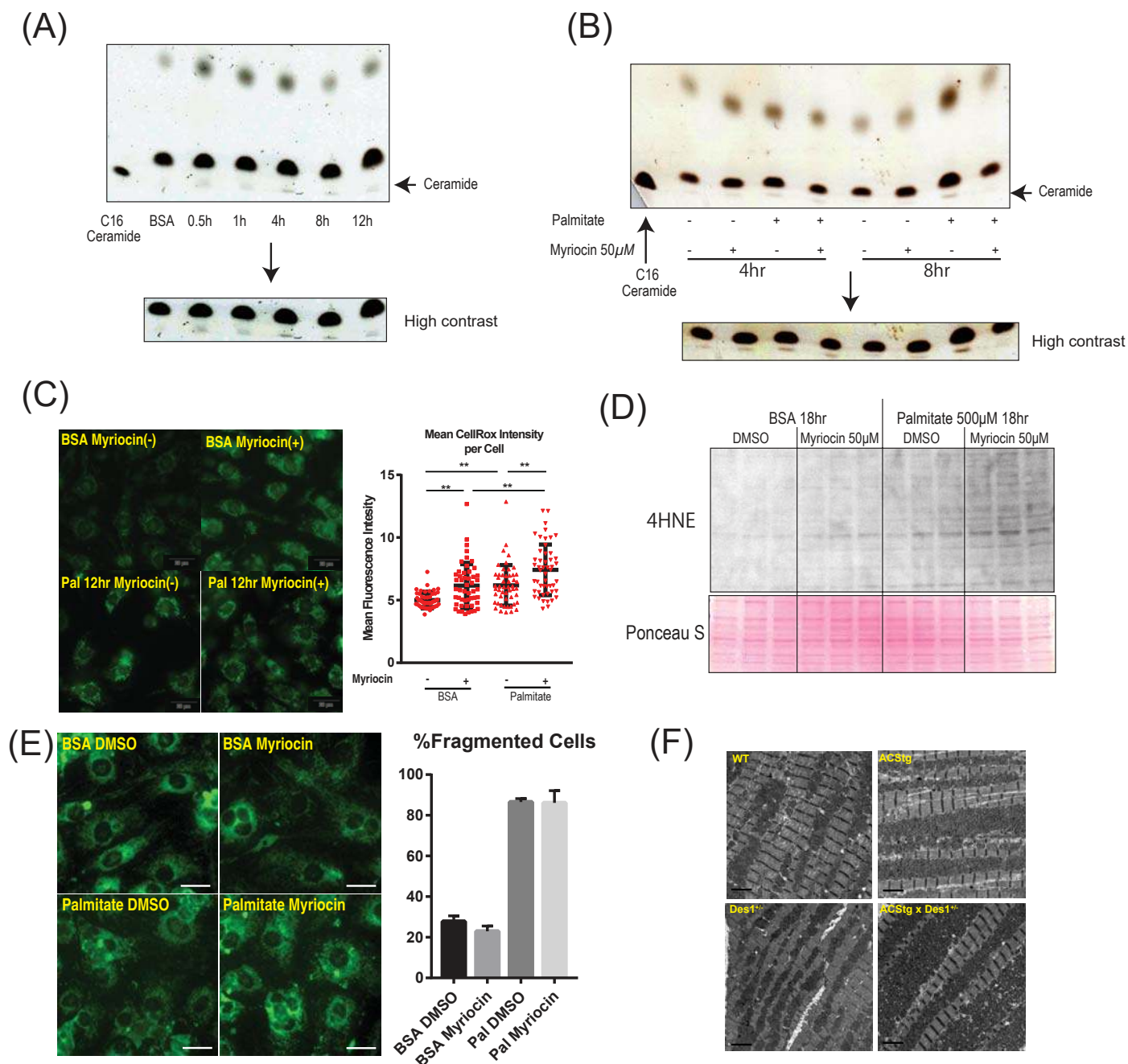


(A) Cardiolipin composition in mitochondrial membranes isolated from 12 week-old WT and ACStg hearts measured by mass spectrometry (LC-MS/MS); n=6.

(B) Content of phosphatidylcholine (PC), phosphatidylethanolamine (PE), phosphatidylserine (PS), and sphingomyelin (SM) in mitochondrial membranes of 12 week-old WT and ACStg hearts measured by thin-layer chromatography; n=6.

Data in (A) and (B) are expressed as fold change relative to WT, which was set to 1 (dashed line). * p<0.05 vs. WT

Supplemental Figure X

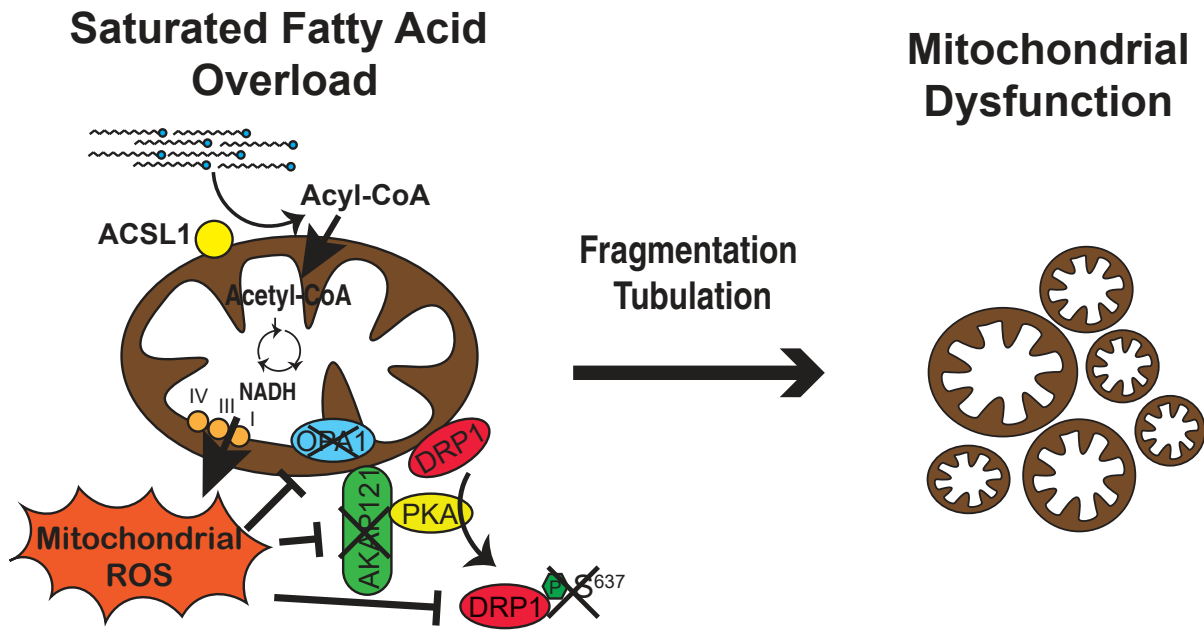


De novo ceramide synthesis inhibition does not rescue mitochondrial fragmentation after lipid overload

(A) Lipids were extracted from NRVCs treated at the indicated time points after palmitate treatment and separated by thin layer chromatocraphy (TLC). Lipids were visualized with sulfuric acid spray. Lane 1 is C16-ceramide control and arrow indicates the position of ceramide. **(B)** Lipid was extracted from NRVCs by chloroform/methanol (2:1) and separated by TLC. Myriocin inhibited the increase in ceramide level after palmitate treatment. **(C)** ROS production in NRVCs were visualised with CellROX green reagent (Thermo Fisher Scientific). ROS production was significantly increased after palmitate treatment. The blockade of ceramide de novo synthesis by myriocin enhanced ROS production. Scale bars indicate 20μm. **(D)** The synthesis of 4-HNE protein adducts were enhanced in myriocin treated groups. **(E)** Mitochondria were immunostained with an anti-Tom20 antibody. Representative images of NRVCs incubated in culture medium supplemented with BSA or 500μM palmitate in the presence or absence of 50μM myriocin, and quantification of fragmented mitochondria. Scale bars indicate 20μm. **(F)** Representative electron micrographs of longitudinal sections from 12-week-old wildtype (WT), ACStg, Des1^{+/-} and ACStg x Des1^{+/-} hearts. Inhibition of the ceramide de novo synthesis pathway could not rescue mitochondrial fragmentation and proliferation in ACStg hearts. Scale bars indicate 2μm.

Supplemental Figure XI

Cardiac Lipotoxicity



Myocardial lipid overload, by saturated fatty acids, transiently increases mitochondrial respiration and ATP generation. Prolonged exposure to lipids increases mitochondrial ROS that modifies Drp1 and OPA1 to impair mitochondrial dynamics and function in the heart, contributing to cardiac hypertrophy and dysfunction.